Atmospheric Research xxx (2012) xxx–xxx

Contents lists available at SciVerse ScienceDirect

Atmospheric Research

journal homepage: www.elsevier.com/locate/atmos

A-Train observations of deep convective storm tops

Martin Setvák [a,*], Kristopher Bedka [b], Daniel T. Lindsey [c], Alois Sokol [d], Zdeněk Charvát [a], Jindřich Šťástka [a,e], Pao K. Wang [f]

[a] Czech Hydrometeorological Institute, Praha, Czech Republic
[b] Science Systems & Applications, Inc., NASA Langley Research Center, Hampton, VA, USA
[c] NOAA/NESDIS/RAMMB, CIRA/CSU, Fort Collins, CO, USA
[d] Faculty of Mathematics, Physics and Informatics, Comenius University Bratislava, Slovakia
[e] Faculty of Mathematics and Physics, Charles University, Praha, Czech Republic
[f] University of Wisconsin-Madison, Madison, WI, USA

ARTICLE INFO

Article history:
Received 20 January 2012
Received in revised form 18 June 2012
Accepted 18 June 2012
Available online xxxx

Keywords:
Convective storm
Storm-top
Overshooting top
Cold-ring shape
Cold-U shape
Enhanced-V feature
Lower stratosphere
A-Train, CloudSat
CALIPSO
MODIS

ABSTRACT

The paper highlights simultaneous observations of tops of deep convective clouds from several space-borne instruments including the *Moderate Resolution Imaging Spectroradiometer* (MODIS) of the Aqua satellite, *Cloud Profiling Radar* (CPR) of the CloudSat satellite, and *Cloud-Aerosol Lidar with Orthogonal Polarization* (CALIOP) flown on the CALIPSO satellite. These satellites share very close orbits, thus together with several other satellites they are referred to as the "A-Train" constellation. Though the primary responsibility of these satellites and their instrumentation is much broader than observations of fine-scale processes atop convective storms, in this study we document how data from the A-Train can contribute to a better understanding and interpretation of various storm-top features, such as overshooting tops, cold-U/V and cold ring features with their coupled embedded warm areas, above anvil ice plumes and jumping cirrus. The relationships between MODIS multi-spectral brightness temperature difference (BTD) fields and cloud top signatures observed by the CPR and CALIOP are also examined in detail to highlight the variability in BTD signals across convective storm events.

1. Introduction

Among the remote sensing platforms used for research purposes or operational monitoring of deep convective clouds (often referred to as "convective storms" hereafter), weather satellites play an important role, either as a complementary data source to radar observations, as a primary data source for monitoring storm development and location in areas with insufficient or no radar coverage, or for detailed studies of storm top structure and temporal evolution. While weather radars provide detailed information on storm 3D structure and dynamics, they are typically unable to detect the details of storm tops, namely those parts or features that are composed of smaller ice particles. Studies performed several decades ago documented that the characteristics of convective cloud tops in weather satellite imagery can be used to infer information about storm intensity, possible severity or internal structure (Purdom, 1976; Adler and Fenn, 1979).

Though our knowledge of convective storm characteristics and dynamics has increased significantly since these early studies through the use of multispectral data from various low-Earth orbit and geostationary satellites in combination with cloud-resolving numerical modeling, many observed features near or above the storm top require further study. Among the various storm-top characteristics and features, several are essential for subjective or automatic identification/detection of potentially severe storms. In addition, a thorough understanding of the relationship between

* Corresponding author at: CHMI, Na Šabatce 17, CZ-14306 Praha 4, Czech Republic. Tel.: +420 606880246; fax: +420 244032442.
E-mail address: setvak@chmi.cz (M. Setvák).

0169-8095/$ – see front matter © 2012 Elsevier B.V. All rights reserved.
doi:10.1016/j.atmosres.2012.06.020

convective cloud vertical structure and satellite observations of cloud top are important for the development and tuning of various derived products such as cloud-top pressure/height (Minnis et al., 2008) and rainfall rate estimates (Rodriguez and Marcos, 2010). In this study we focus on the following features:

- overshooting cloud tops;
- cold-U/V and cold-ring features with their embedded warm areas;
- above-anvil ice plumes and jumping cirrus;
- characteristics of the brightness temperature differences (BTDs) between a water vapor (WV) absorption band and an infrared (IR) window band above convective storm tops.

Overshooting tops (OTs, see Bedka et al., 2010 and references therein) represent a strong updraft at the upper levels of convective storms and their characteristics (e.g. height and temporal persistence) has been related to storm severity (Dworak et al., 2012). Though many studies have addressed the OT feature, their cloud top height were either inferred based on shadows they cast (van Hees et al., 1999) or derived indirectly using stereographic observation methods (Hasler, 1981; Negri, 1982; Mack et al., 1983). In our study we use the A-Train data (described below) not to provide a statistically significant survey of OT characteristics, but rather to show the importance of very fine co-location and parallax correction of A-Train data in the evaluation of OT magnitude. We also briefly address the variability in cloud-top height within OT regions derived from various A-Train datasets.

Closely related to OTs is another category of features, cold-U/V signatures, (or alternatively referred to as enhanced-V, see Negri, 1982; Fujita, 1982; McCann, 1983; Heymsfield et al., 1983a), cold ring signatures (Setvák et al., 2010; Putsay et al., 2011), and the embedded warm areas within the U/V and ring signatures (first documented by Mills and Astling, 1977). These storm-top features observed in IR imagery are known to be well correlated with severe weather (McCann, 1983; Adler et al., 1985), so automatic detection algorithms are currently being developed for nowcasting applications (Bedka et al., 2011; Iršič Žibert and Žibert, this issue). Though several explanations have been proposed for the formation of these storm-top features (Heymsfield et al., 1983b; Schlesinger, 1984, 1988; Adler et al., 1985; Adler and Mack, 1986; Heymsfield and Blackmer, 1988; Heymsfield et al., 1991; Wang, 2007), certain ambiguities still exist. These ambiguities primarily concern the interpretation of the embedded warm area inside the cold U/V feature. Explanations for the warm areas include non-adiabatic processes associated with either OT collapses or wave-like flow across the OT region, lower cloud-top heights within the warm areas, and cloud-top microphysics which impacts the IR transparency or emissivity. In reality, some of these processes most likely combine to form various types of embedded warm areas. In the present study, we document how A-Train data can contribute to a better understanding of these features, showing one case of storm exhibiting a distinct cold-U shape and another with a distinct cold-ring feature.

"Above-anvil ice plumes" gained their presently used name from analyses of AVHRR imagery (Levizzani and Setvák, 1996), but had been documented much earlier in studies based on GOES observations (e.g. Fujita, 1982; Adler et al., 1983) and aircraft observations (Fujita, 1982), and more recently simulated in cloud-resolving model studies (e.g. Wang, 2007). Observations indicate (Fujita, 1982; Mack et al., 1983) that these plumes may contribute to the formation or appearance of the warm area inside cold-U/Vs by a "plume masking mechanism" (Setvák and Rabin, 2003). One of the goals of this study is therefore to use A-Train data to document the detailed vertical structure of the plumes, as well as their link to the warm area inside the cold-U/V feature. Similarly, A-Train data should be capable of detecting "jumping cirrus" (Fujita, 1982), a phenomenon very similar to the above-anvil ice plumes and possibly with a similar impact on the cloud-top brightness temperature (BT). Here we show one case of distinct jumping cirrus near an active OT.

The BTD between a WV absorption band and an IR window band within convective storm tops has been documented since the mid-1990s (Fritz and Laszlo, 1993; Ackerman, 1996; Schmetz et al., 1997). Despite numerous papers on the subject, many ambiguities still persist in the interpretation of this BTD. A positive BTD value can result either from the presence of warmer water vapor above the storm top, or from scattering/emissivity effects in thin cirrus at or above the cloud top (Lattanzio et al., 2006). In this paper we use A-Train observations to highlight these ambiguities and attempt to better understand BTD observations using radiative transfer simulations.

The National Aeronautics and Space Administration (NASA) A-Train satellite constellation (http://atrain.nasa.gov/, Stephens et al., 2002) offers a unique opportunity to study the details of storm tops mentioned above, utilizing data from several satellites and their various instruments. These (among others) include the Aqua satellite with its *Moderate Resolution Imaging Spectroradiometer* (MODIS, http://modis-atmos.gsfc.nasa.gov/), CloudSat with its *Cloud Profiling Radar* (CPR, http://cloudsat.atmos.colostate.edu/), and the CALIPSO satellite with its *Cloud-Aerosol Lidar with Orthogonal Polarization* (CALIOP, http://www-calipso.larc.nasa.gov/), *Wide Field Camera* (WFC), and *Imaging Infrared Radiometer (IIR)*. The satellites within the A-Train constellation orbit in very close proximity to one another, providing near-simultaneous observations of convective cloud tops from a diverse array of active and passive sensors at 1:30 AM/PM local time. The A-Train data sets are complemented in this study by geostationary weather satellite observations such as the Meteosat Second Generation (MSG) *Spinning Enhanced Visible and Infrared Imager* (SEVIRI) and the National Oceanic and Atmospheric Administration (NOAA) Geostationary Operational Environmental Satellites (GOES).

2. Data sources, processing and satellite data visualization

2.1. Data sources and processing

2.1.1. MODIS and MSG SEVIRI

Aqua MODIS and MSG SEVIRI provide observations of convective cloud tops via reflected sunlight and multispectral IR radiances. The radiances are converted into BTs within each of the available spectral channels that then can be differenced from one another to provide additional information about clouds. In this paper we use only a small subset of the MODIS bands: band 1 (centered at 0.65 μm), band 5 (1.24 μm), band 7 (2.11 μm), band 27 (6.7 μm), band 30 (9.7 μm), band 31 (11.0 μm) and band 36 (14.2 μm). Of particular interest to this study is the BTD between

Please cite this article as: Setvák, M., et al., A-Train observations of deep convective storm tops, Atmos. Res. (2012), doi:10.1016/j.atmosres.2012.06.020

the WV absorption channel (centered at 6.7 μm on MODIS and 6.2 μm on SEVIRI) and ~11 μm IR window channel (see Setvák et al., 2008 and references therein).

Aqua MODIS Level 1B radiances (MYD021KM) and 1 km navigation files (MYD03) were acquired from the NASA Level 1 and Atmosphere Archive and Distribution System (LAADS, http://ladsweb.nascom.nasa.gov/). The original MODIS Level 1B 5-minute granules were destriped and merged together (when needed) utilizing a combination of the University of Wisconsin Space Science and Engineering Center's International MODIS AIRS Processing Package (IMAPP, http://cimss.ssec.wisc.edu/imapp/) and the command line tool "hrepack" (http://www.hdfgroup.uiuc.edu/HDF4/doctools/hrepack/hrepack.html). The MSG SEVIRI data used in this paper were retrieved from the EUMETSAT Data Center archive system (https://eoportal.eumetsat.int/). The BT color enhancement used in this paper complies with that recommended by the EUMETSAT's Convection Working Group (http://www.convection-wg.org/). The MODIS and SEVIRI imagery were visualized by the ENVI software. Final tuning and editing of the images presented below was done mainly in the Adobe Photoshop.

2.1.2. CloudSat

The CloudSat CPR reflectivity factor product (2B-GEOPROF, Stephens et al., 2002; Mace et al., 2007) was used in combination with CALIOP data (described below) to examine the vertical structure of convective cloud tops. The CPR is an active sensor that emits and detects reflected microwave energy at a frequency (wavelength) of 94 GHz (3.2 mm). Given the wavelength of the CPR pulse, the CPR signal often penetrates through the small particles typically present near the cloud top. As a result, the uppermost height of the returned CPR signal will often be below than that observed by a lidar instrument such as the CALIOP. The footprint of a CPR profile covers 1.7 km in the along-track direction and 1.3 km in the across-track direction. A new profile is captured every 1.1 km, indicating that there is some overlap between adjacent profiles (i.e. oversampling). The effective vertical resolution is 480 m, with oversampling at 240 m resolution. The 2B-GEOPROF product provides a cloud mask and radar reflectivity at each of the 125 vertical data bins. A reader is directed to the CloudSat Data Products Handbook (see References section) for additional detail on CloudSat and the 2B-GEOPROF product. The CPR data were acquired from the CloudSat Data Processing Center (http://www.cloudsat.cira.colostate.edu) and visualized using CCPLOT from Peter Kuma (http://ccplot.org/).

2.1.3. CALIPSO

CALIPSO combines an active lidar instrument with passive infrared and visible imagers to probe the vertical structure and properties of clouds and aerosols. Three datasets from the CALIPSO satellite were used in this study: the CALIOP, WFC, and IIR. The CALIOP emits and receives backscattered energy at 532 and 1064 nm wavelengths. CALIOP features a pulse repetition frequency of 20 Hz, yielding a horizontal resolution of 333 m. Given the higher spatial resolution and the sensor wavelength(s), CALIOP can detect clouds with a lower optical depth than the CloudSat CPR. Moreover, CALIOP also detects even smaller aerosol particles, which escape CPR detection entirely.

The WFC is a fixed, nadir-viewing imager with a single spectral channel covering the 620–670 nm region, selected to match band 1 of the MODIS instrument on Aqua. The WFC collects data at 125 m spatial resolution with a swath width of 5 km, and at 1 km resolution from a swath 61 km wide. Similarly, the IIR provides calibrated radiances at 8.65, 10.6, and 12.05 μm at 1 km spatial resolution over a 64 km swath centered on the lidar footprint. Given that the WFC, IIR and CALIOP collect simultaneous observations, the combination of these datasets allows one to better interpret the CALIOP backscatter signal. The CALIOP backscatter, IIR and WFC data used in this paper were acquired from the NASA Langley Research Center Atmospheric Science Data Center (http://eosweb.larc.nasa.gov/) archive and visualized using the CCPLOT or ENVI software.

2.1.4. Aura

Aura is the last of the A-Train satellites we use in our study. It flies about 8 min behind the other A-Train satellites, sampling the atmosphere with four instruments. One of these is the Microwave Limb Sounder (MLS) from which profiles of upper tropospheric and stratospheric temperature and various other atmospheric constituents can be derived. The along-track sounding of MLS is performed by the instrument aimed ahead of the satellite, at the limb area approximately under the actual position of the remaining A-Train satellites. Given the limb profiling nature of the measurement, the spatial resolution is on the order of 5 km cross-track × 500 km along track × 3 km vertical, thus the MLS profiles provide an indication of the general character of the environment in a broader sense than a rawinsonde. In this study, we use the MLS temperature and humidity profiles in addition to the standard soundings. The MLS data used in this study were acquired from the NASA Goddard Earth Sciences Data and Information Services Center (GES DISC) archive. The vertical plots of these data were visualized using our own Interactive Data Language routine.

2.2. Description of the blended "sandwich" image product

When studying certain storm-top features in satellite imagery, it is essential to know their spatial arrangement in various spectral bands or advanced products based on these bands. The most typical example is the comparison of storm-top appearance in a visible band with the IR-window brightness temperature (BT) field — e.g. when studying characteristics of the overshooting tops, various BT features (such as cold-U/V or cold ring phenomena), above-anvil plumes, etc. One possibility is comparing the images "side--by-side" (such as in Fig. 1A–D, or 3A–F of this paper), or alternatively fast toggling of the images in various bands forward and backward (usable only on a computer, not in a printed form).

A more desirable and visually appealing option is blending ("sandwiching") the images together, using one of the blending functions available in some of the graphics editors (such as Adobe Photoshop (http://www.adobe.com/photoshop.html), GIMP (www.gimp.org), or Image Magick (www.imagemagick.org/)). The blended product ("sandwich") consists of two layers: the base layer, which is usually one of the visible or near-IR bands at the best pixel resolution as possible, and the upper layer, containing a field such as the

Please cite this article as: Setvák, M., et al., A-Train observations of deep convective storm tops, Atmos. Res. (2012), doi:10.1016/j.atmosres.2012.06.020

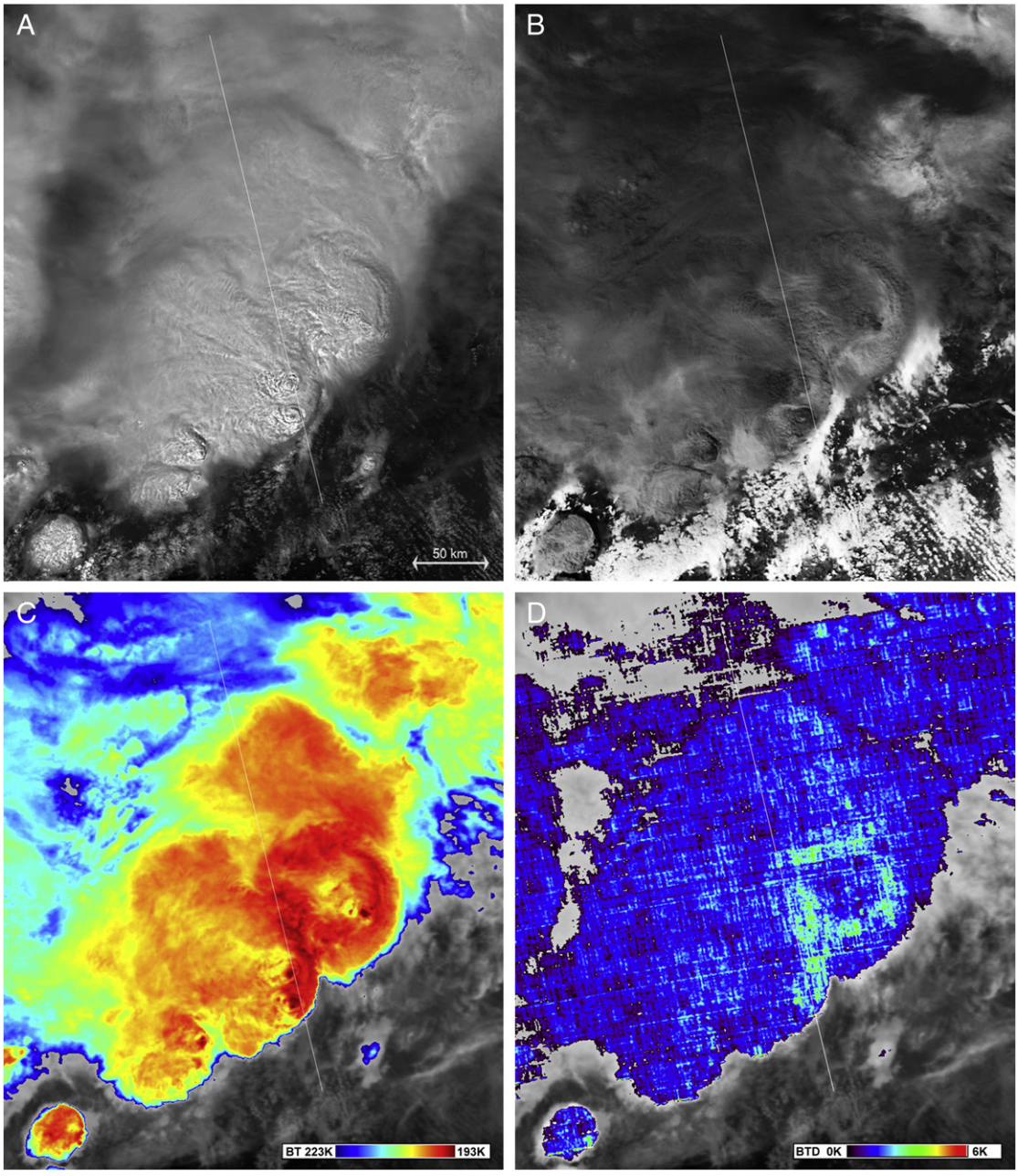

Fig. 1. a–d. 2007/05/06, 19:28 UTC, MODIS/Aqua. Convective storms above Missouri, U.S.A. (center of the storms ~39 N/93 W). Fig. 1a (top left) — band 1 image, Fig. 1b (top right) — band 7 image, Fig. 1c (bottom left) — color enhanced band 31 image (blue—223 K, red — 193 K), and Fig. 1d (bottom right) — brightness temperature difference image of bands 27 and 31. White line indicates the CALIPSO/CALIOP scan line as based on CALIPSO WFC data. e. Blended ("sandwich") product of the 250 m band 1 (Fig. 1a) and color-enhanced band 31 (Fig. 1c), showing these storms in detail. The white lines show the scan tracks of CloudSat/CPR and CALIPSO/CALIOP — the left line as based on LAT/LON information from HDF data, the right line as based on WFC data; crosses indicate ground locations of these at five-second intervals. f. Comparison of the scan tracks of CALIOP as based on the LAT/LON information from CALIOP data (in MODIS image the left line) and as determined from the WFC image (in MODIS image the right line, and in WFC image the red line). The WFC image consists of 1 km data (outer parts of the swath) and 125 m data (narrow area in the center of the swath). g. CALIPSO CALIOP (Total Attenuated Backscatter at 532 nm, top) and CloudSat CPR (bottom) profiles of the storms above. h. Springfield sounding for the case above. i. MLS limb sounding in the area of the storms above. Left plot shows the temperature profile and right plot the moisture profile (volume mixing ratio).

color-enhanced IR-window image remapped to the same map projection and pixel resolution as the visible band. There are several options to blend these two image layers together. The most simple method is to use partial transparency applied to the upper layer, setting the layer opacity somewhere between 40% and 75%. Much better results can be obtained by using a more advanced type of blending of the two layers together — for example in Adobe Photoshop the "Multiply" or "Linear Burn" functions, again in combination with the upper layer opacity.

Please cite this article as: Setvák, M., et al., A-Train observations of deep convective storm tops, Atmos. Res. (2012), doi:10.1016/j.atmosres.2012.06.020

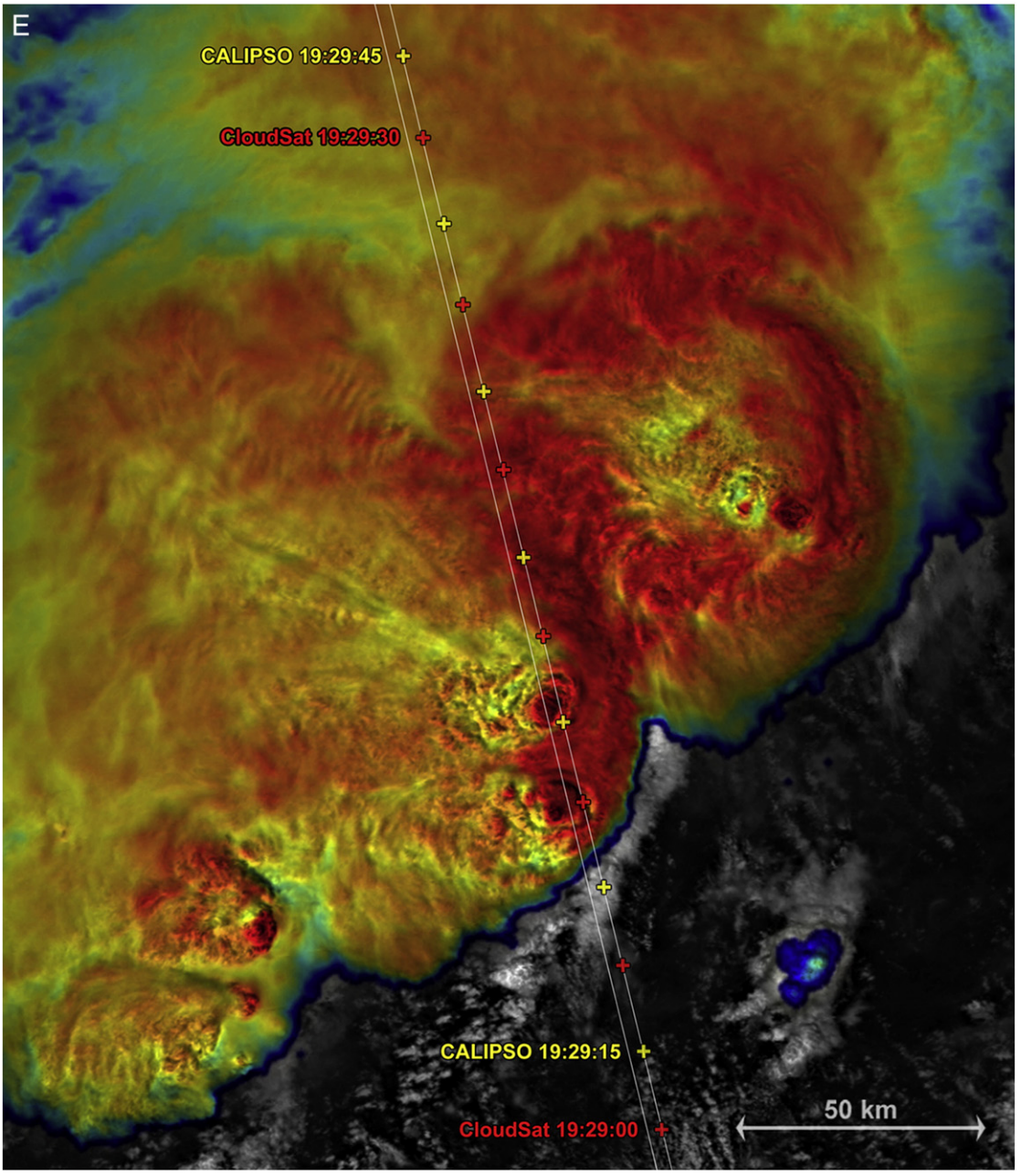

Fig. 1 (*continued*).

The main advantage of such sandwich products is that they merge the features of the two input images into one single image, thus enabling one to observe the characteristics of both images simultaneously in one single product. In the case of the visible–IR-window sandwich combination, the visible band brings to the final image the cloud-top "morphology" (shadows and textures), while the color--enhanced IR-window band adds the BT information. Such images often gain almost a 3D appearance, which is absent if the source input images are compared side-by-side. Such blended products become even more attractive when used in satellite image loops.

In this paper we present only the "standard" sandwich product — the combination of visible (MODIS band 1) and IR-window (band 31) images; however, the sandwich product can be modified in many other ways — by replacing the IR-window band by any other band or their combinations (e.g. RGB composites).

3. Data characteristics and general remarks

An initial challenge in the processing and visualization of datasets from the three satellites was accurate, very precise co-location. The main reason for this is the fact that most of

Please cite this article as: Setvák, M., et al., A-Train observations of deep convective storm tops, Atmos. Res. (2012), doi:10.1016/j.atmosres.2012.06.020

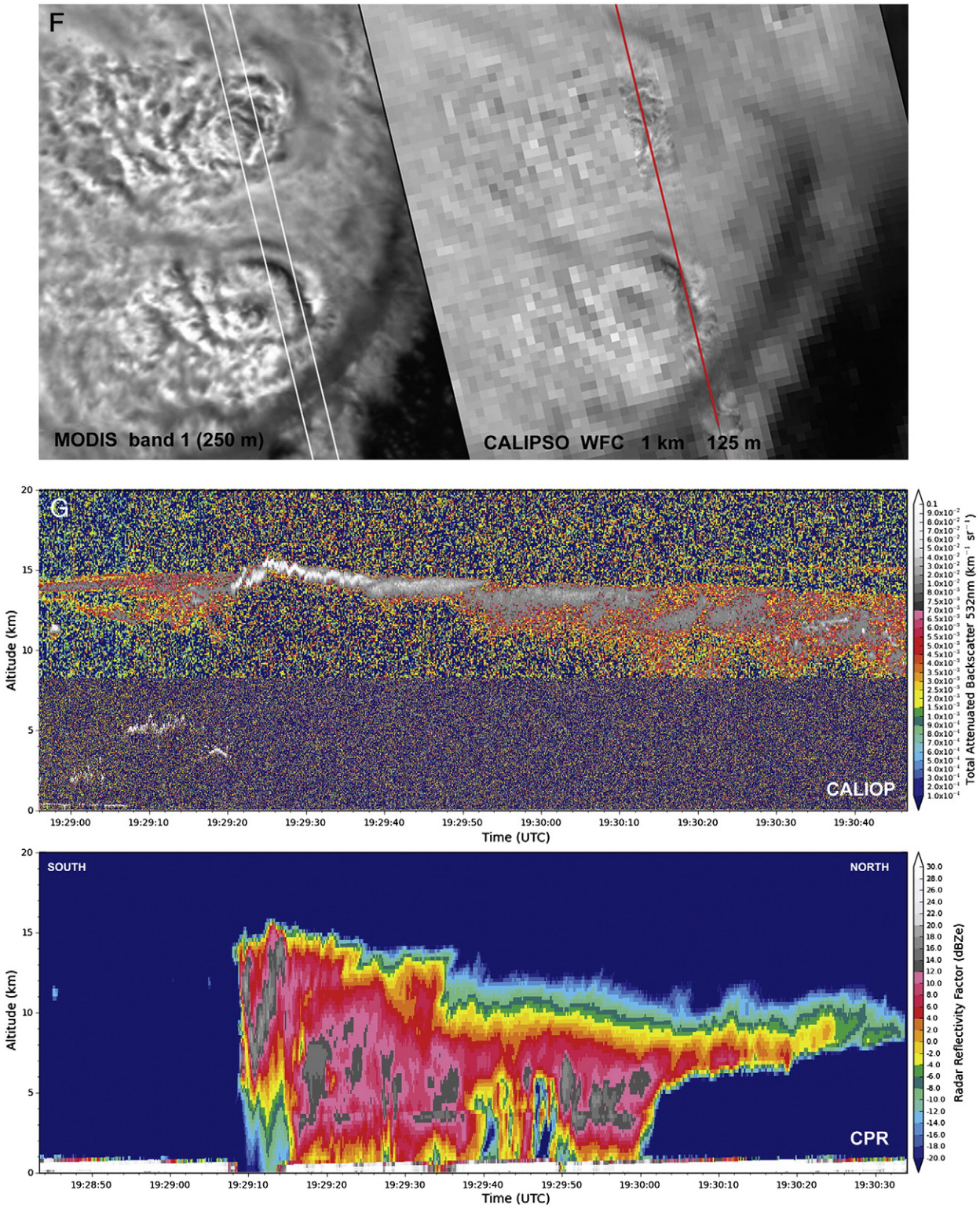

Fig. 1 (*continued*).

Please cite this article as: Setvák, M., et al., A-Train observations of deep convective storm tops, Atmos. Res. (2012), doi:10.1016/j.atmosres.2012.06.020

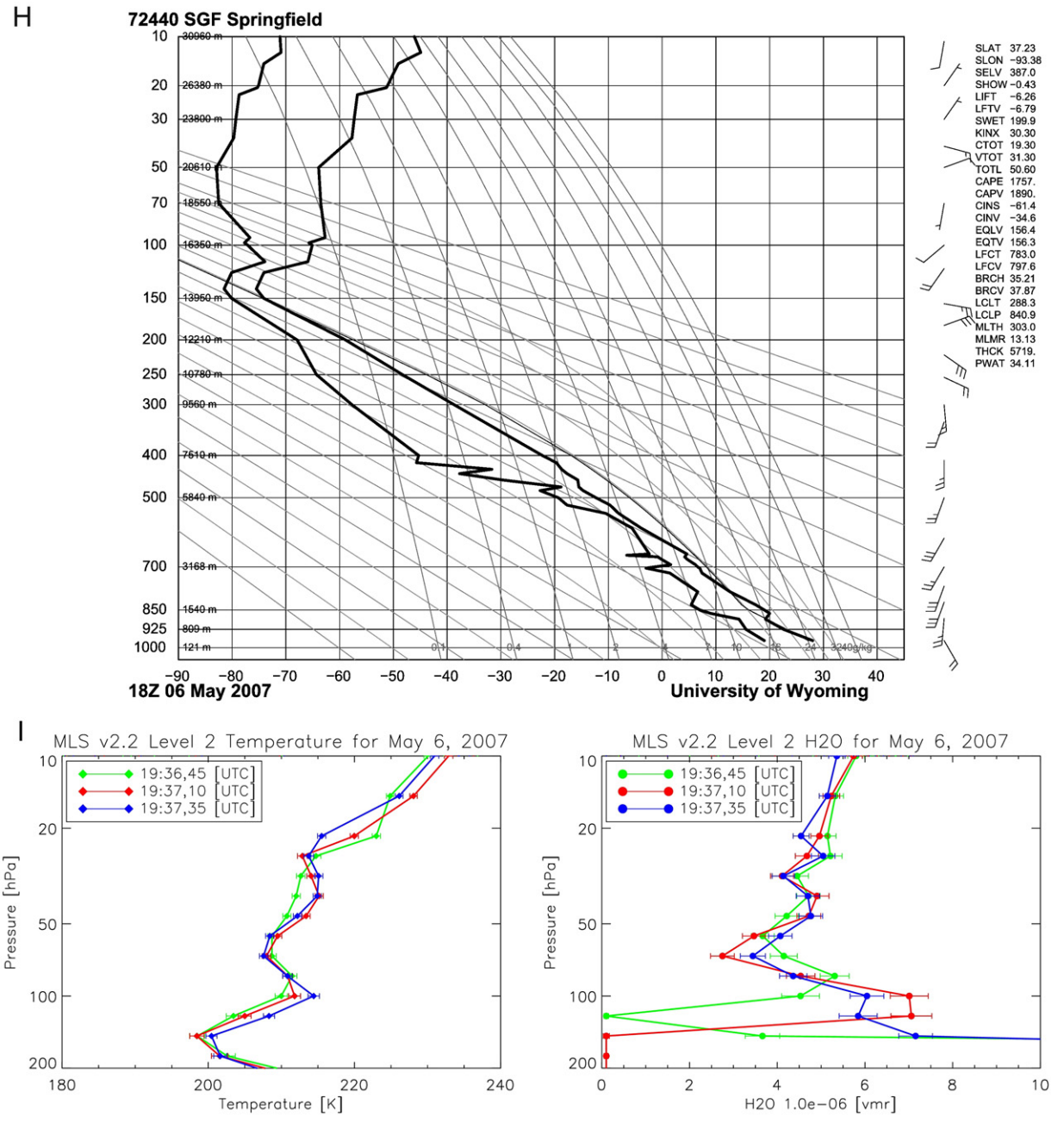

Fig. 1 (*continued*).

our features of interest are of small size, often on the order of several km across, thus their mutual identification and co-location in all the datasets have to be very accurate to avoid misinterpretation. It is important to note that the ground tracks (and namely their timestamps) of CloudSat and CALIPSO when plotted atop the MODIS data need to be based on the LAT/LON information included in the CloudSat 2B-GEOPROF and CALIPSO CALIOP HDF data, as plotting the tracks of these two satellites based on the North American Aerospace Defense Command (NORAD) two-line element orbital data was found to be inaccurate for the purposes of this study, resulting in a shift of the timestamps along the track on the order of several seconds. The reason for this is the fact that the two instruments do not sample exactly at nadir; both are slightly tilted in order to achieve timing of their sampling as close as possible.

Another step required to properly co-locate MODIS, CALIPSO, and CloudSat CPR observations is adjustment of the data to account for the MODIS parallax shift. Parallax is a well-known issue for geostationary satellite datasets (Joyce et al., 2001), but this must also be taken into account when dealing with MODIS data. When deep convective cloud tops with heights of 15–20 km are observed by MODIS that orbits the Earth at a 705 km altitude, parallax causes a displacement

Please cite this article as: Setvák, M., et al., A-Train observations of deep convective storm tops, Atmos. Res. (2012), doi:10.1016/j.atmosres.2012.06.020

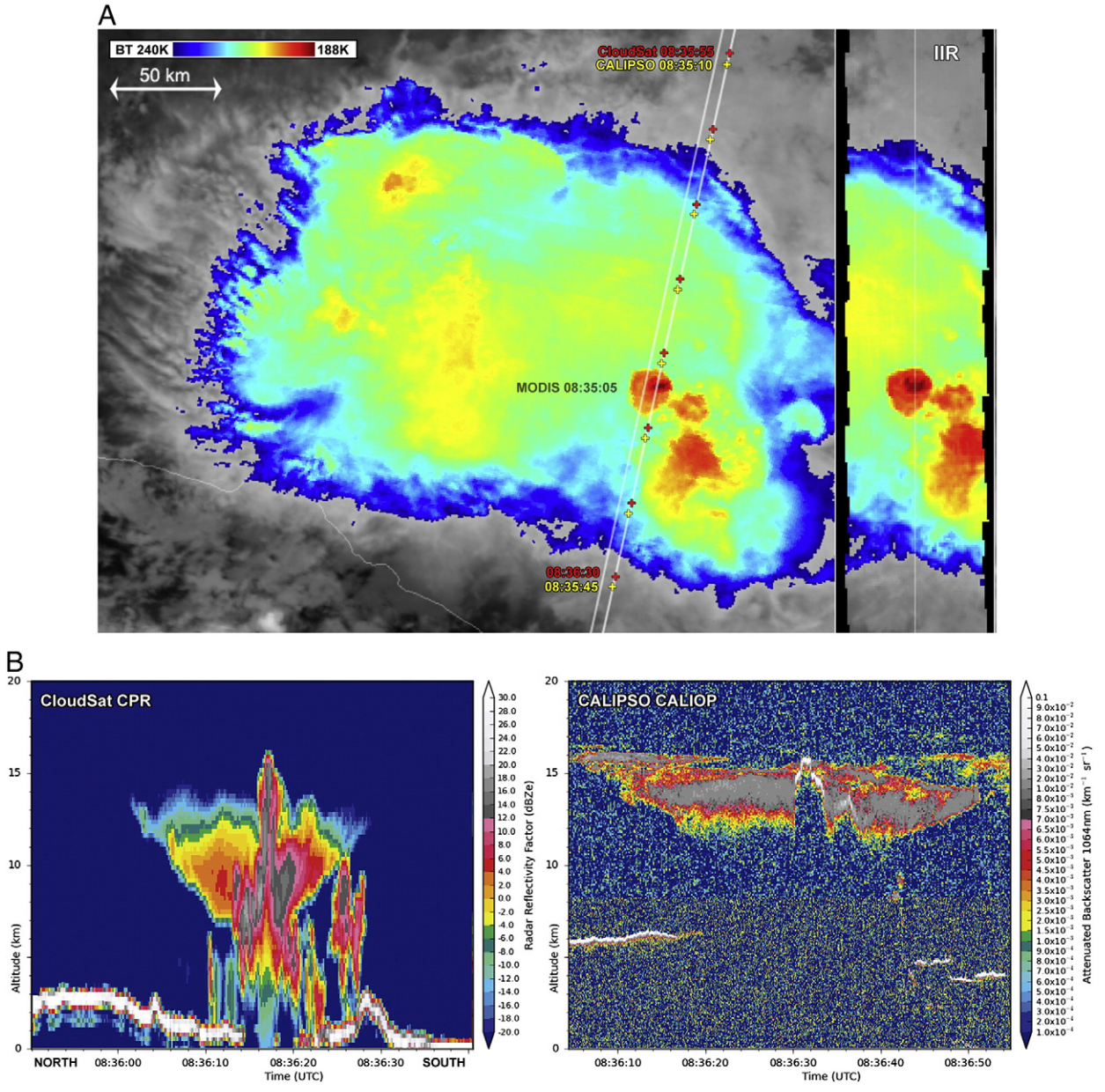

Fig. 2. A. 2007/07/16, 08:35 UTC, MODIS/Aqua, color-enhanced band 31. Nocturnal storms above central-west Mexico (about 18 N/100 W). The white lines show the scan tracks of CloudSat/CPR and CALIPSO/CALIOP — the left line as based on LAT/LON information from the CPR/CALIOP data and the right line as based on the IIR data; crosses indicate ground locations of these at 5-second intervals. The color-enhanced IIR 10.6 μm band swath is shown at right, with the white line indicating the center of the swath. B. CloudSat CPR (left image) and CALIPSO CALIOP Total Attenuated Backscatter at 1064 nm (right) profiles of the storm from Fig. 2.

of 3–5 km from their true Earth-relative location (at the distance from sub-satellite track, where the CloudSat and CALIPSO sample the storms). In principle, there are two possible ways to correct (shift) the ground-track to eliminate the parallax shift. One possible approach is to compute the parallax shift, based on the cloud-top height (retrieved from the CPR or CALIOP data) and the MODIS viewing zenith angle for the area of interest. Another possibility is to shift the HDF-data-based CALIOP track to match the center lines of the WFC or IIR swaths. All the tracks shown in this paper utilize one of these parallax-correction methods that will be cited when each of the selected storm events is described.

Though the A-Train satellites provide data with an unprecedented degree of synchronization, the time difference between Aqua MODIS and CloudSat observations can approach two minutes, which can be problematic when comparing overshooting top observations from these two instruments. The authors' personal experience analyzing numerous cases of one-minute resolution super-rapid scan observations from GOES (see the following for examples: http://cimss.ssec.wisc.edu/goes/blog/?s=SRSO) or five-minute rapid scan data of the MSG, coupled with the aircraft-based analysis of Shenk (1974) indicates that an individual overshooting top may persist for less than 5 min. Thus, it is entirely

Please cite this article as: Setvák, M., et al., A-Train observations of deep convective storm tops, Atmos. Res. (2012), doi:10.1016/j.atmosres.2012.06.020

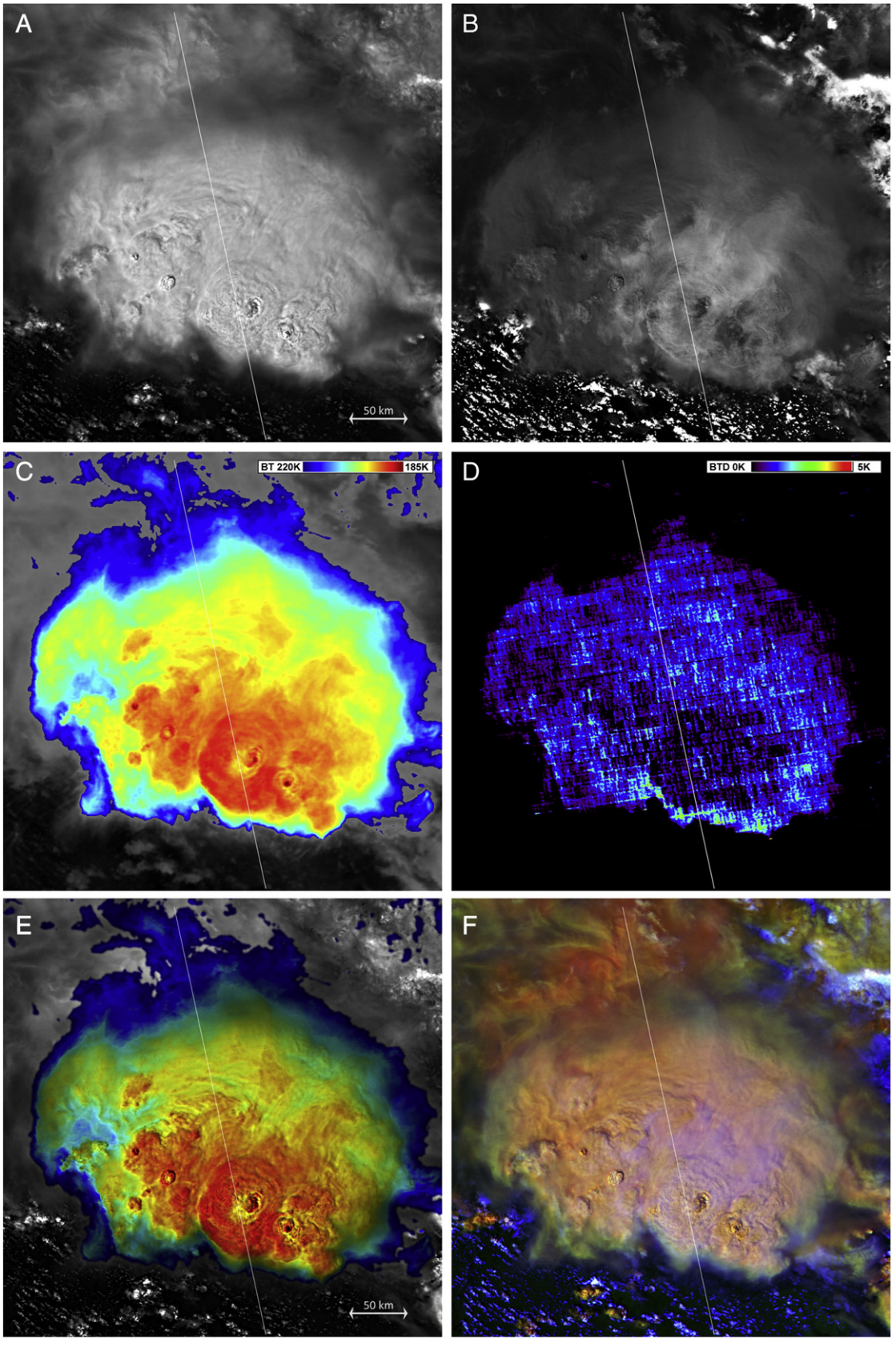

Please cite this article as: Setvák, M., et al., A-Train observations of deep convective storm tops, Atmos. Res. (2012), doi:10.1016/j.atmosres.2012.06.020

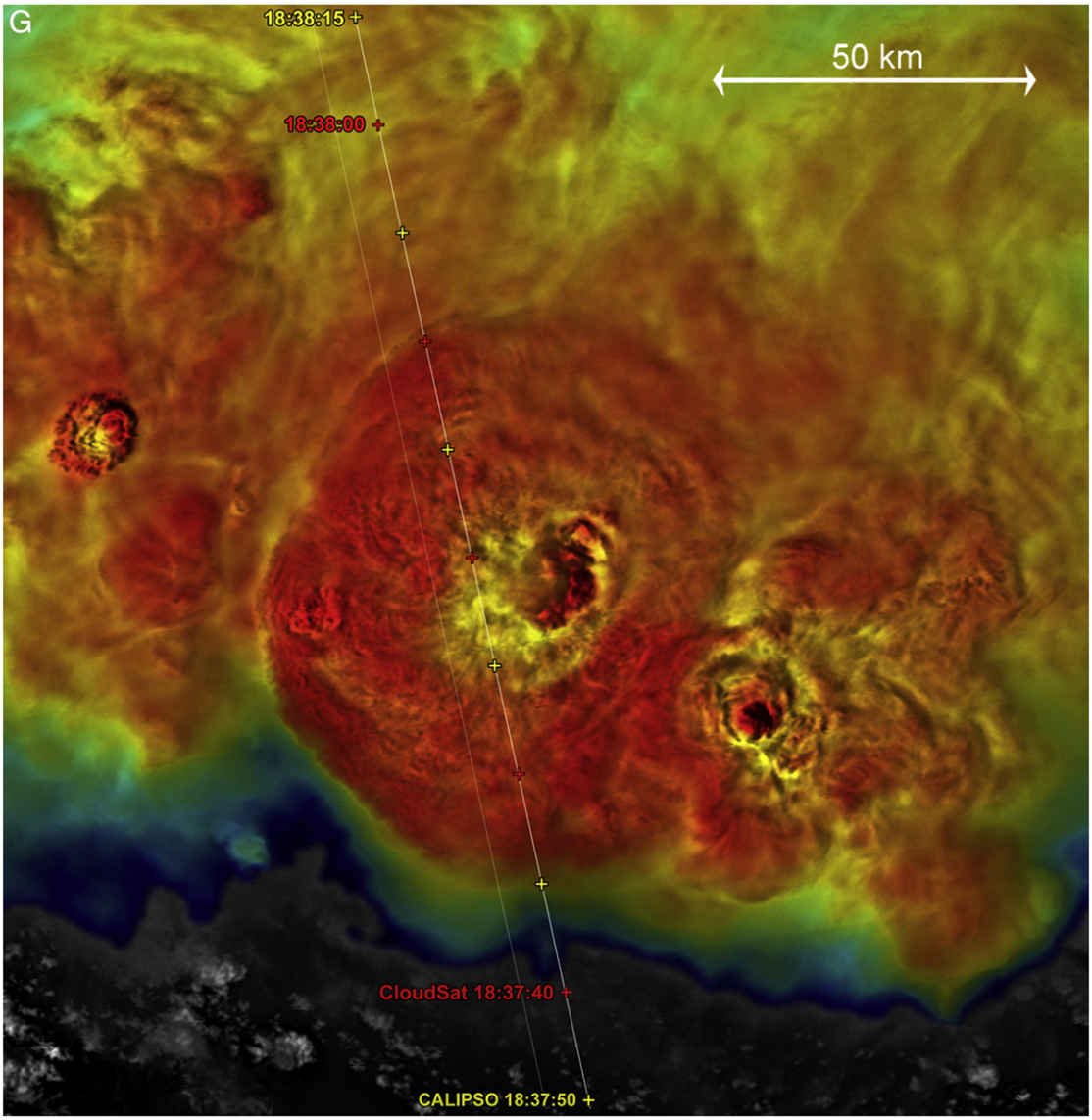

Fig. 3. A–D. 2007/12/22, 18:37 UTC, MODIS/Aqua — storms above west Brazil (about 9S, 72W). Fig. 3a — band 1 (top left); Fig. 3b — band 7 (top right); Fig. 3c — color-enhanced band 31 (bottom left); and Fig. 3d — BTD of bands 27 and 31 (bottom right). White line indicates the CALIPSO/CALIOP scan line as based on CALIPSO WFC data.E–F. Fig. 3e — sandwich product of band 1 and color-enhanced band 31 (left); Fig. 3f — RGB product of bands 1, 5 and 7 (right).G. Blended ("sandwich") product of the 250m band 1 and the color-enhanced band 31 BT, showing in detail the very fine structures of the storms. The white lines show the scan tracks of CloudSat/CPR and CALIPSO/CALIOP — the left line as based on LAT/LON information from HDF data, the right line as based on WFC data; crosses indicate CALIOP and CPR scan time at five-second intervals.H. Profiles of the upper levels of the storms: CALIOP (blended Total Attenuated Backscatter at 532 and 1064nm, top), CloudSat CPR reflectivity (middle), and blended product of these two (bottom). Black lines outline the extent of the cold ring as based on the MODIS data; white lines mark the thin material extending upwards in the CALIOP data, which matches exactly the faint plume streaming westward from the OT (see Fig. 3g); and the red lines indicate a very faint material seen in the CALIOP profile, which corresponds to the higher band 7 reflectivity material seen north of the cold ring (Fig. 3b).

possible that the MODIS data could depict a significant overshooting top signature that had either grown or decayed by the time of the CloudSat observation. This was not necessarily an issue for the cases analyzed in this paper but should be considered in future studies.

Another challenge for this study was the difference in time between the A-Train overpass and the peak intensity and coverage of convective storms. In general, deep convective storms typically only begin to develop at the time of the early afternoon (1:30 PM local time) A-Train overpasses, thus the chance of detecting a well-developed convective storm is rather low at mid-latitudes. Somewhat better is the chance of detecting mature storms during the midnight overpasses; however many of these storms at this time are decaying or have already attained mesoscale convective system characteristics, which often do not have the distinct storm-top features of interest to this study. Given the small size of the features addressed by this study, even if the A-Train overpass

Please cite this article as: Setvák, M., et al., A-Train observations of deep convective storm tops, Atmos. Res. (2012), doi:10.1016/j.atmosres.2012.06.020

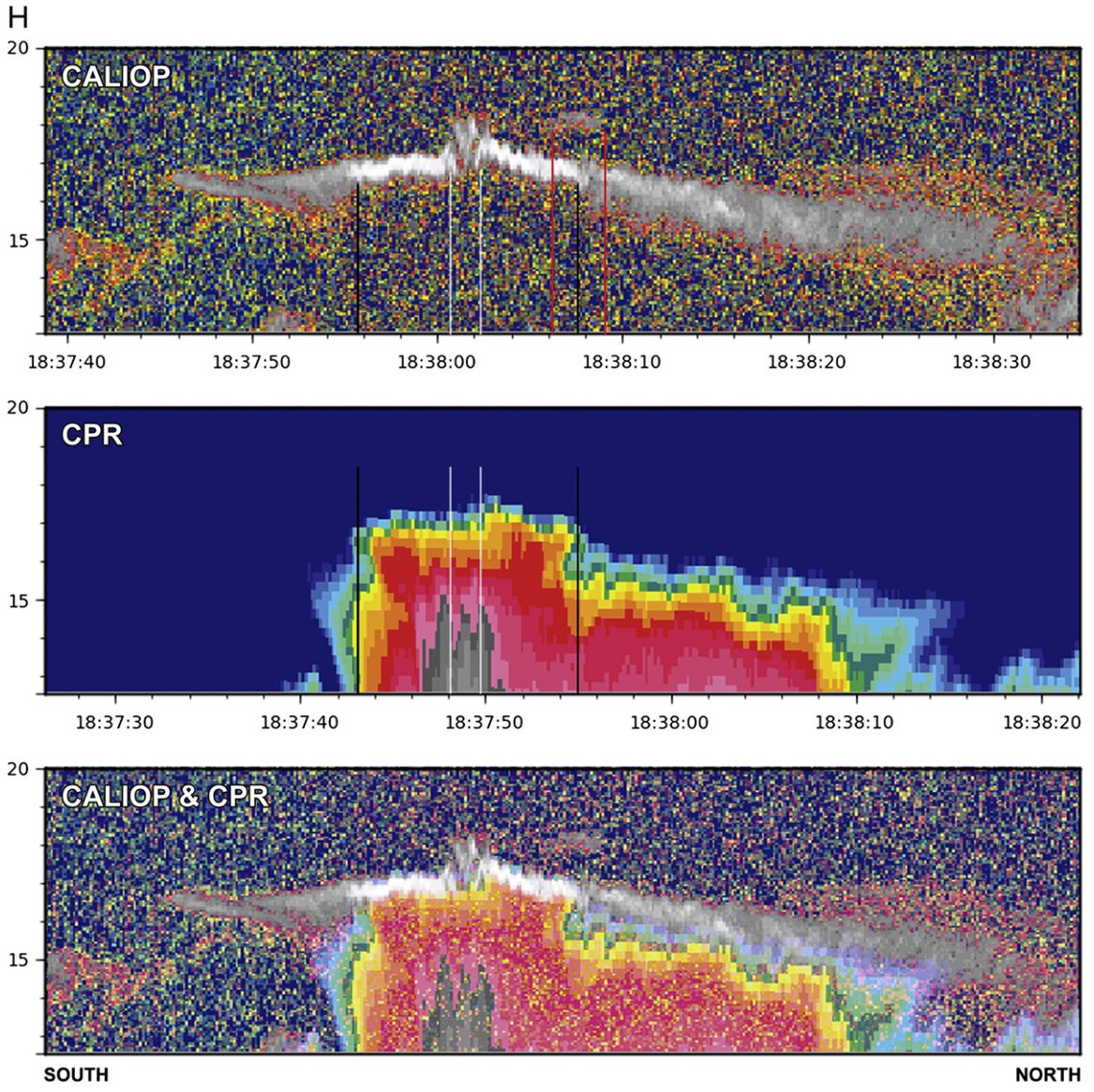

Fig. 3 (*continued*).

intersects a mature storm, it most often misses the features of interest. Therefore, the five cases described below represent the most interesting cases we found so far, after examining a total of about 80 cases from 2006 to 2010. It should be noted that most of the ~80 cases examined within this study did not show any of the features of interest listed in the Introduction, with the exception of overshooting tops, which can be found more frequently in the CloudSat and CALIPSO data than the other features (Bedka et al., in press).

4. Selected convective storm events observed by the A-Train

4.1. Missouri, 06 May 2007

Fig. 1A–D shows MODIS observations of several storms over the central U.S. at 19:28 UTC on 6 May 2007. The feature that first attracted our attention was the prominent cold-ring (Setvák et al., 2010) seen in the MODIS band 31 atop of one of the storms near the CloudSat and CALIPSO track (Fig. 1C). Although the track missed the cold ring itself, the case is still interesting from several other aspects.

The plot of the original CloudSat CPR and CALIPSO CALIOP tracks based on the LAT/LON information retrieved from the HDF data (see the left lines on the MODIS images in Fig. 1E and F) indicated that the two instruments should have scanned two distinct overshooting tops (OT). However, only one weak OT-like feature appears in the CPR (at 19:29:13 UTC) and CALIOP profiles (at 19:29:25 UTC), shown in Fig. 1G. This discrepancy can be explained after applying the parallax shift correction of the track, in this case using the WFC swath images. The Level 1 WFC swath data (right panel Fig. 1F) is misaligned by ~400 m relative to the CALIOP track (personal communication with Dr. Michael Pitts of NASA Langley Research Center, 2012), so the track in the WFC

Please cite this article as: Setvák, M., et al., A-Train observations of deep convective storm tops, Atmos. Res. (2012), doi:10.1016/j.atmosres.2012.06.020

125 m image (red line) is shifted by this amount to the left of the swath center line. The result is that the corrected track does not directly intersect both OTs and now samples the edge of the northernmost OT. This explains why we do not see these distinct OTs in the CPR and CALIOP profiles, but instead only a small trace of one OT. This case illustrates that the parallax shift has to be considered when using the A-Train data for detailed studies of overshooting tops.

Another interesting aspect of this case is the appearance of the BTD field atop these storms using MODIS band 27 minus band 31 (henceforth "BTD" unless stated otherwise, Fig. 1D). The literature would suggest that BTD values should be near 0 or slightly positive in convective anvil cirrus clouds and significantly positive (>~2 K) in OT regions (see description in Section 5). In this case, the opposite of traditional conceptual model is evident in that highly positive BTD values are present throughout the cold ring signature and other cirrus anvil cloud pixels, but no significant values are present in the OT regions. The general BTD pattern is closely correlated with the band 31 BT field.

One of the general possible explanations for the positive BTD values within cirrus anvil clouds is variability in cloud-top microphysics. As the cloud-top microphysics is closely related to cloud-top reflectivity in the 1.6–4 μm bands, it is possible to compare the BTD field to one of these "microphysical" bands when searching for explanation of the observed positive BTD values. Among the MODIS microphysical bands, band 7 (Fig. 1B) provides probably the best combination of high sensitivity to the cloud-top microphysics, high pixel resolution (500 m), and minimal striping, which are the main reasons why we use this particular MODIS band within this study. Higher reflectivity portions of the cloud top shown in light gray or white in the MODIS band 7 reflectance field (Fig. 1B) correspond to the small ice particles, while the dark shades correspond to larger particles. The BTD field matches the band 7 reflectivity

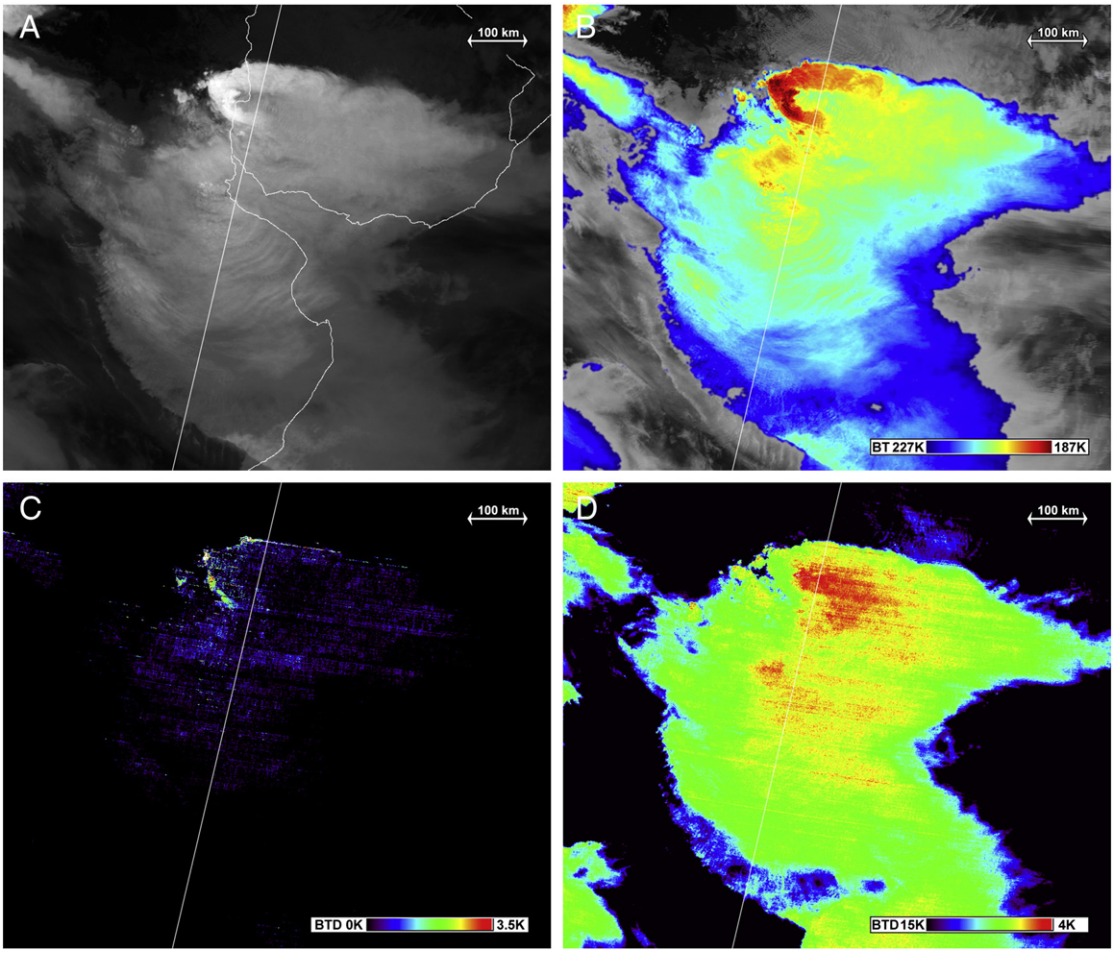

Fig. 4. A–D. 2009/12/23, 05:16 UTC, MODIS/Aqua. Convective storms above Argentina and Uruguay (center of the storms about 33 S/58 W). Fig. 4a (top left) — band 31 image (slightly enhanced, with coastlines and political borders); Fig. 4b — color enhanced band 31 (range of the enhancement: 187 K (dark blue)–227 K (dark red)); Fig. 4c — BTD image of bands 27 and 31 (range of the enhancement: 0 K (black)–3.5 K (red)), and Fig. 4d — BTD image of bands 30 and 36 (range of the enhancement: 15 K (black)–4 K (red)). White line shows the track of CALIPSO. E. Detail of the same storm as above — black and white enhanced band 31 image, range of the enhancement: 185 K (white)–215 K (black). The white line and five-second marks show the CALIOP track after parallax correction based on the IIR swath data, the arrows (labeled A–I) indicate the individual areas as shown in the CALIOP profile (Fig. 4f). F. CALIOP Total Attenuated Backscatter 532 nm profile of the storm along the line shown in the Fig. 4e. For a detailed discussion of the profile see the text. G. Meteosat-9 (MSG-2) SEVIRI view of the same storm, at 05:18 UTC (about two minutes after the MODIS image). Left: MSG SEVIRI color-enhanced band IR10.8 (same color enhancement as for the MODIS band 31, above). Right: BTD of MSG SEVIRI bands WV6.2 and IR10.8, range 0 K–8.5 K (different color enhancement range than for the MODIS BTD b27–b31).

Please cite this article as: Setvák, M., et al., A-Train observations of deep convective storm tops, Atmos. Res. (2012), doi:10.1016/j.atmosres.2012.06.020

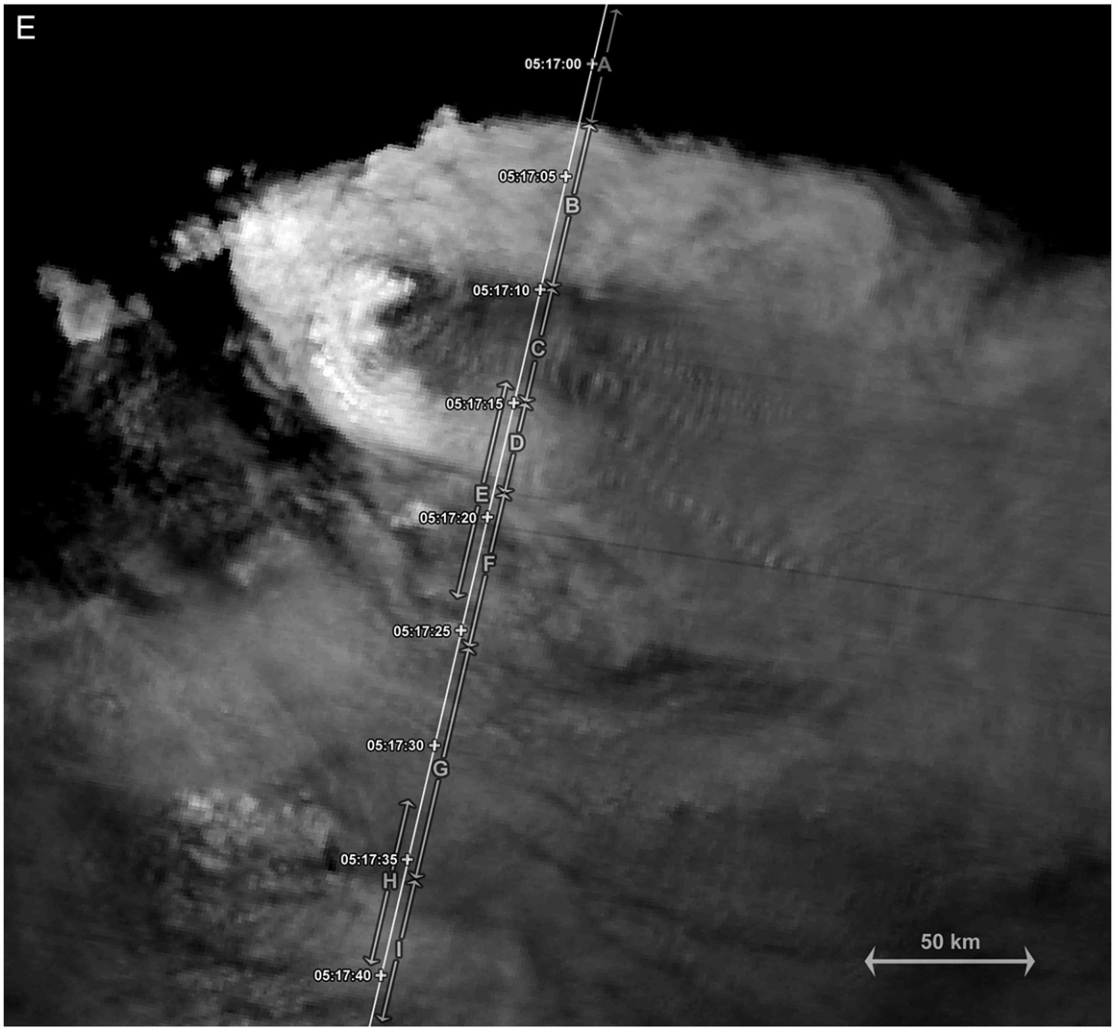

Fig. 4 (*continued*).

pattern only very loosely, indicating that the storm-top microphysics cannot account for the BTD field appearance. The BTD for this case is analyzed and discussed in greater detail in Section 5.

4.2. Mexico, 16 July 2007

A nocturnal convective storm event over west-central Mexico at 08:35 UTC on the 16 July 2007 (Fig. 2) first attracted our attention mainly because of the apparently extremely high overshooting top in the CloudSat CPR profile (Fig. 2B, left). This case features a situation opposite of the case above, where it would appear that the CPR and CALIOP HDF-data-based track passed over the western part of the OT, missing the coldest pixels in the MODIS IR data. However, the parallax-shifted track (based on IIR L2 swath) indicates that these instruments sampled the coldest pixels and presumably highest peak of the OT.

While the anvil cloud surrounding the aforementioned CPR-observed OT reaches about 14 km, the CALIOP profile shows the cloud top at about the 15.5–16 km level, which is approximately the same height as the top of the OT. This nicely documents the differing nature of these two instruments — CPR detects larger particles that are often deeper within the cloud and CALIOP detects much smaller ones at the upper fringe of the cloud. In this case, a new storm cell developed within the anvil of an older decaying storm (confirmed by GOES data, not shown here) that is composed of thin material at its upper levels. This calls into question the definition of a "cloud top" in that the height of a "cloud top" strongly depends on the instrument that observes the cloud (Mace et al., 2009). This point should be considered when using the CloudSat and CALIPSO data for verification of various derived products, such as cloud top height or for OT studies. The following examples (Sections 4.3 and 4.5) nicely show that in the case of mature storms with optically dense anvil cloud, the cloud tops observed by both instruments are in much better agreement within the active parts of the storms.

4.3. Brazil, 22 December 2007

This tropical cold-ring shaped storm from 22 December 2007 (18:37 UTC) over western Brazil (Fig. 3) is the first one (and so far the only one among the 80 cases examined in

Please cite this article as: Setvák, M., et al., A-Train observations of deep convective storm tops, Atmos. Res. (2012), doi:10.1016/j.atmosres.2012.06.020

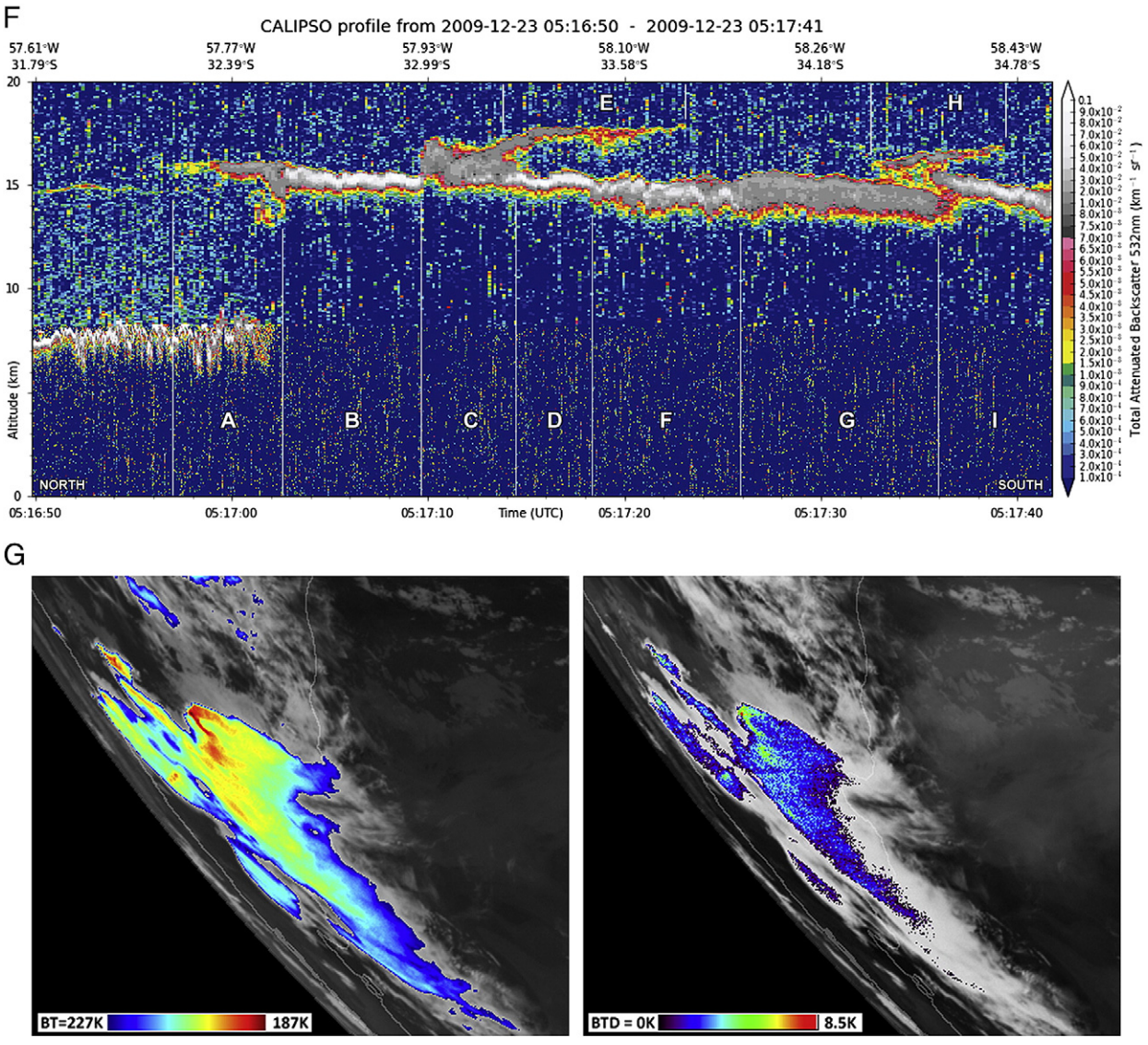

Fig. 4 (*continued*).

preparation for this study) where the CloudSat and CALIPSO instruments profile the embedded warm area (central warm spot (CWS)) inside the cold ring. Also, this is the first storm exhibiting a cold ring documented in the tropics so close to the Equator (about 9°S) in peer-reviewed literature.

Comparing the MODIS appearance of the storm (Fig. 3A–G) with CPR and CALIOP profiles (Fig. 3h) instantly shows that the cloud top is at the same height for both instruments within the area of the cold ring (in the profiles indicated by the black vertical lines). The only and the most important difference between these can be found in the core of the cold ring (inside the white lines in the profiles). While the CALIOP profile shows a “fountain-like” feature in the center of the cold ring area, there is no trace of it in the CPR profile. This means that this feature is composed of smaller ice particles, detectable by CALIOP but invisible to CPR. Comparing the timing of this CALIOP feature with the track in a detailed sandwich product image of the cold ring (Fig. 3G) shows that this feature does not match with the entire CWS, but only with a smaller part of it, where the track crosses a thin plume-like feature streaming west of the OT center. This plume can be better seen in the high-resolution sandwich zoom of the storm (Fig. 3G) based on the 250 m MODIS band 1, but not as clearly in the other lower-resolution images (Fig. 3A–F) due to its size and faint nature. Another interesting aspect is that the cloud top within the cold ring signature is slightly higher north of the storm core than south, but this doesn't seem to have any effect on the cloud top temperature.

South of the cold ring (Fig. 3H, outside the black line to the left of the storm core) CALIOP shows only a thin anvil cloud that is missing in the CPR profile. North of the ring (right in the profiles) the cloud top resembles the previous case, with the CPR-based cloud top being lower than that in

Please cite this article as: Setvák, M., et al., A-Train observations of deep convective storm tops, Atmos. Res. (2012), doi:10.1016/j.atmosres.2012.06.020

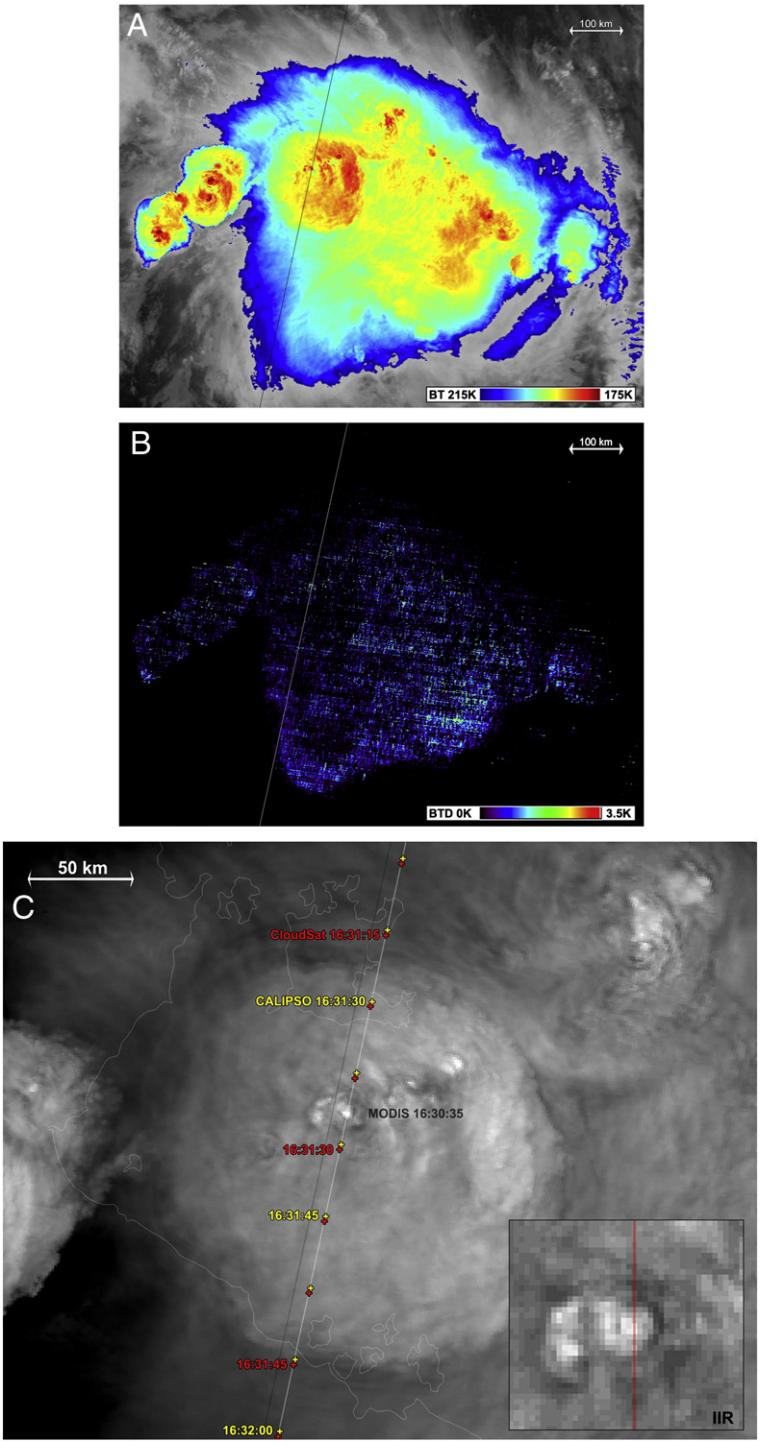

Fig. 5. A–B. 2010/01/26, 16:31 UTC, MODIS/Aqua; nocturnal convective storms above northern Australia (center of the main storm about 15 S/137E). Fig. 5a (left): color-enhanced band 31 (enhancement range 175 K (red)–215 K (dark blue)). Fig. 5b (right): BTD (b27–b31) of the same storm, BTD range 0 K–3.5 K. The line shows the CloudSat/CPR and CALIPSO/CALIOP track after applying the parallax shift correction (based on IIR swath). C. Detail of the main storm from Fig. 5a. Dark line shows the original HDF-based track, the white line and 5 s marks the same track after the parallax correction (IIR-based). The insert at bottom right shows a zoomed crop of the IIR 10.6 swath (L2 swath data), with its center-line crossing exactly the most prominent overshooting top of this storm. D. CALIPSO CALIOP Total Attenuated Backscatter 532 nm (top) and CloudSat CPR (bottom) profiles of the storm above (Fig. 5a). The insert in the top panel shows the overshooting top area using slightly different enhancement and vertical stretch; the arrow points to possible jumping cirrus that is clearly visible in the CALIOP lidar data, but entirely missing in CPR data.

Please cite this article as: Setvák, M., et al., A-Train observations of deep convective storm tops, Atmos. Res. (2012), doi:10.1016/j.atmosres.2012.06.020

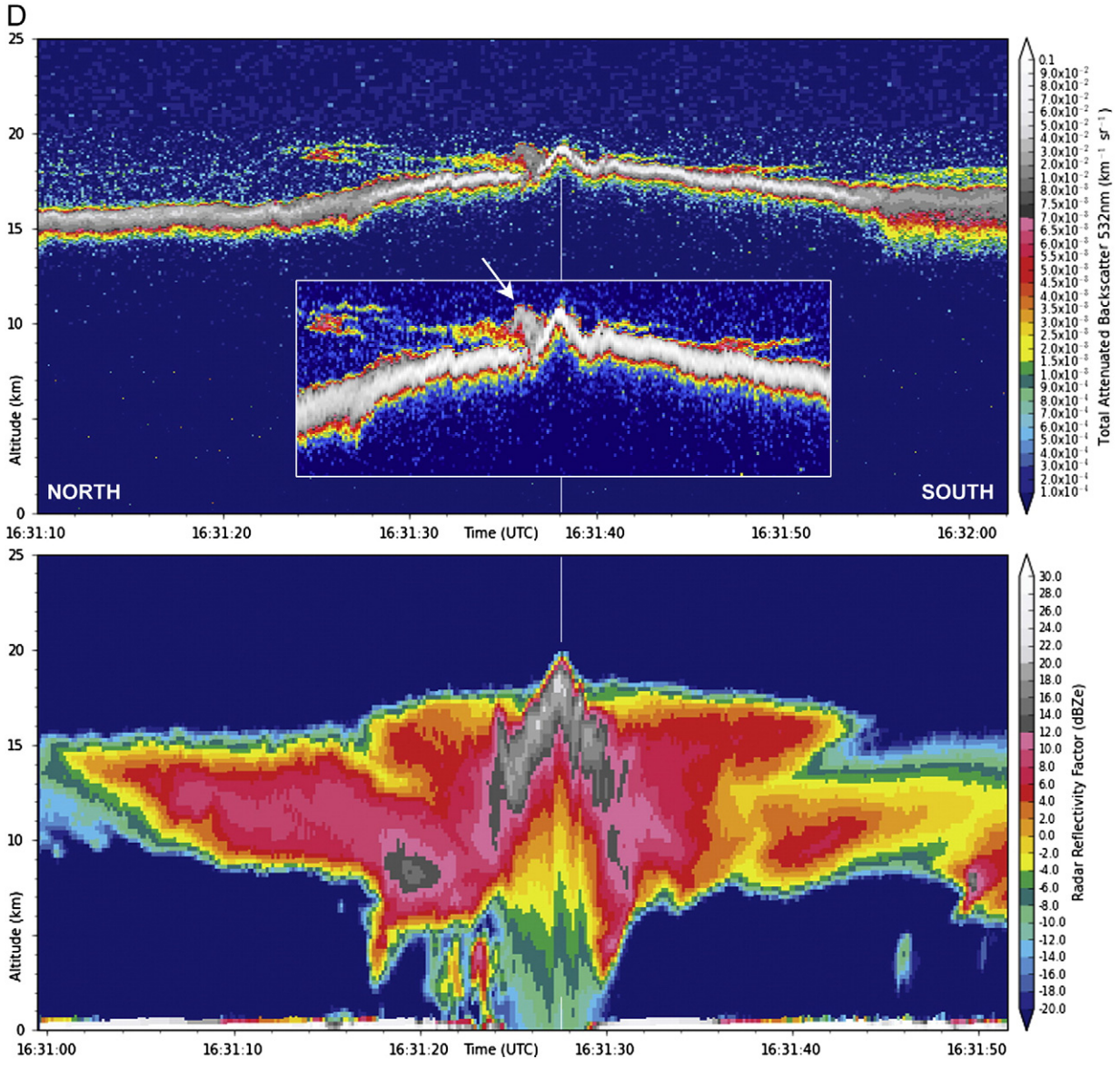

Fig. 5 (*continued*).

the CALIOP profile. This means that the cloud top is composed of smaller particles here in the upper levels of the anvil. This is partially in agreement with the MODIS band 7 appearance of the storm top (Fig. 3B) — just north of the cold ring is a broad "plume" of higher reflectivity material (shown white in band 7), spreading from the cold ring area to the northeast. The same higher-reflectivity material can be seen in the RGB composite image of bands 1, 5 and 7 (Fig. 3F) as whitish against the darker-yellow rest of the storm top. The profiles also show that this optically thinner material slopes down gradually, while the CPR-based cloud top "jumps" down north of the cold ring. This band 7 reflectivity decreases quickly (dark gray in band 7, brownish in the RGB composite image) at about 18:38:20 UTC (of the CALIOP profile), approximately at the same area where the CPR reflectivity also weakens significantly.

The smaller dim patch of higher CALIOP reflectance indicated by the red lines seems to correspond to the higher band 7 reflectivity material seen at the north edge of the cold

Table 1
Radiative transfer model simulation results of the 6.8 μm BT, 11 μm BT, and 6.8–11 μm BTD (in K) based on the 18 UTC Springfield, Missouri sounding for three scenarios described in the paper text.

	6.8 μm	11.0 μm	6.8–11.0 μm
Base case	200.483	199.711	0.772
Enhanced WV	200.642	199.711	0.931
Thin cloud	201.636	201.013	0.623

Please cite this article as: Setvák, M., et al., A-Train observations of deep convective storm tops, Atmos. Res. (2012), doi:10.1016/j.atmosres.2012.06.020

ring. This feature showed up well only in a combined product of both lidar bands (532 and 1064 nm), which to a certain degree reduces the higher noise present in the daytime CALIOP data. In Fig. 3H, a blended image of the two bands assembled in Photoshop is also shown.

Another very interesting aspect of this case is the character of the BTD field. It is quite opposite to that of the first (Missouri) case. The BTD values with the cold ring signature are very low but they increase outside the cold ring above the warmer portions of the storm. In addition, a comparison of the BTD and band 7 reflectivity indicates that cloud-top microphysics can probably be excluded as the mechanism behind the BTD because the two fields do not correlate here. The reason for this atypical character of the BTD field remains unanswered for now.

4.4. Argentina–Uruguay, 23 December 2009

Probably the most important and interesting case of this study occurred during the night of 23 December 2009 at 05:16 UTC over the Argentina–Uruguay border. Fig. 4 shows a textbook storm with a cold-U shape in the band 31 image (Fig. 4A and B), with CALIPSO crossing almost perpendicular to both cold arms of the U-shape, as well as the close-in warm area (CWA) inside the cold arms. Fig. 4E shows this storm in detail, together with the CALIOP track (IIR-corrected) and its segments as labeled in the CALIOP profile (Fig. 4F). Unfortunately, no CPR data is available for this case, as CloudSat was temporarily down during this period.

The CALIOP profile shows a multi-layer cloud top with a distinct amount of material elevated above the "base" anvil cloud top and a feature resembling a thin plume streaming south (right) of it. The CALIOP profile and the corresponding MODIS image shown in Fig. 4E can be split into the following segments:

(A) very thin northern edge of the storm anvil. It can't be seen in Fig. 4E due to its higher brightness temperature, resulting from its partial transparency. However, this thin edge can be seen well in various BTDs, tuned to show the thin cirrus (e.g. difference of the MODIS bands 29 and 32, not shown in this paper). A rotor-like feature is present in the profile beneath the cirrus cloud (~16 km) just left of the line between segments A and B; interpretation of this feature is uncertain.

(B) north cold arm of the cold-U feature, with a cloud top of 15.5 km.

(C) the elevated warmer material of the warm area inside the cold arms (also known as the "close-in warm area" (CWA) within literature describing the enhanced-V). The top of this material extends up to about 17 km, and probably is the source of ice particles carried downwind at 17.5–18 km in the form of a very thin plume feature (E).

(D) southern cold arm of the cold-U feature, with its cloud top at 15.5 km, partially covered by the thin plume (E).

(E) very thin plume at 17.5–18 km, vertically separated from the rest of the anvil cloud top underneath. Notice the smaller waves oriented parallel to the track, present above most of the CWA region, as well as within the (E) feature area.

(F), (G) and (I) adjacent parts of other storm cells or anvils south of the cold-U shaped storm, differing by their optical thickness and height (I). These are not of any particular importance for this case, though a gravity wave signature is also evident in the CALIOP profile but not apparent in the MODIS image.

(H) another vertically separated layer of thin cirrus; its origin is uncertain.

The main message of this case is that it proves (at least in this particular case) that the warm area inside the cold arms is much higher than the cold arms themselves, thus situated in warmer layers above the tropopause within the lower stratosphere. The absence of CloudSat data makes it impossible to infer anything about the optical thickness of the storm under this warm area at the levels of the cloud-top of the cold arms. Therefore it is very difficult if not impossible to explain the warmer radiance from this area — does it originate from the elevated material of the area (C), or is the area optically thin enough to enable a thermal contribution from lower, warmer levels underneath? It is most likely that the material which we see within the area (C) may correspond to the above-anvil plume, as its west–east extent can be inferred from the presence of smaller-scale waves atop it (roughly parallel with the track) spreading east of the CALIOP track.

We experimented with various possible BTD combinations of the MODIS bands in an effort to highlight the higher material of area (C), but the only combination that causes this material to appear is a BTD of the absorption bands 30 (O_3) and 36 (CO_2) which is shown in Fig. 4D. The values of this BTD are lowest (shown red) only at the region corresponding to the elevated warm area, and higher for all other parts of the storm, thus are not correlated to the band 31 BT of the cloud top. All other BTD combinations depict the CWA similarly as any other parts of the storm at the corresponding temperature. Testing this specific BTD on other cases did not show any unambiguous link with the cloud top height. Thus, the mechanism behind this particular BTD and the reasoning for why it would clearly depict the CWA is presently unclear and requires further studies.

Fig. 4C shows very low values of the BTD (WV-IRw), with some increase at the anvil edges resulting from a different IR transparency of the thin cirrus there. We show this BTD here namely for comparison with similar BTD based on MSG/SEVIRI data. Fig. 4G documents that the MSG-based BTD (WV6.2-IR10.8) is much higher compared to the MODIS one, most likely as a result of very low scan angle (and thus much longer path of the radiance through the stratosphere). This MSG-based BTD also shows that the BTD closely correlates with the IR10.8 BT, which is the most frequent case for the MSG-based BTDs based on the author's personal experiences. The reason why MSG-based BTDs are typically correlated with the IR10.8 BT, while the MODIS-based ones are much more uncorrelated is presently unclear and will be addressed in future studies.

Please cite this article as: Setvák, M., et al., A-Train observations of deep convective storm tops, Atmos. Res. (2012), doi:10.1016/j.atmosres.2012.06.020

4.5. Australia, 26 January 2010

The final case we document in this paper occurred at night over northern Australia on 26 January 2010 at 16:31 UTC (Fig. 5). The main reason we present this case is the details of the cloud top around its main OT as detected by CALIOP. The CALIOP profile shows that the primary OT extended to a height of almost 20 km, comparable to that observed in the CPR profile which indicates that larger ice particles were present in core of the OT region. A second peak of slightly decreased CALIOP backscatter appears just to the south of the OT (see arrow in Fig. 5D). This feature strongly resembles a breaking gravity wave that can produce a phenomenon known as "jumping cirrus" which was documented more than three decades ago by Fujita (1982), and later modeled by others (e.g. Wang et al., 2009). This is one of the best cases of jumping cirrus observed by CALIOP in our database, where both the vertical and horizontal magnitudes of this phenomenon as well as the adjacent very thin plumes spreading away from the OT area in both directions are clearly evident. The detailed CALIOP image also depicts gravity waves spreading away from the OT that are not apparent in the CPR profile, implying that the waves either had a horizontal wavelength that was too small to be observed by the CPR or that they were shallow and only present at the very top of the anvil cloud. As there are only weak signatures of the gravity waves in the detailed MODIS and IIR images (Fig. 5C), the latter explanations seems more plausible. The BTD field (Fig. 5D) resembles that of the Brazil case — the coldest storm tops exhibiting very low BTD values, with the higher BTD values found above warmer, older parts of the anvil, namely at the southeast sector of the storms.

5. Brightness temperature differences and their link to possible lower stratospheric moisture

Positive values of the BTD between a water vapor absorption band and one of the IR-window bands have for many years been attributed to the presence of a warmer moist layer above cold tops of convective storms (Fritz and Laszlo, 1993; Ackerman, 1996; Schmetz et al., 1997). The source of the warmer LSM was thought to be either advection from remote locations (distant storms), resulting in the BTD field closely matching the IR-window field itself, or injection of the moisture upwards, into the lower stratosphere by the storm itself, resulting in "BTD anomalies" (Setvák et al., 2008; Šťástka and Radová, 2012; Putsay et al., 2012). An example of the BTD (WV-IRw) and its strong correlation with the IRw BT field can be seen by comparing Fig. 1C with Fig. 1D. Note that the largest positive values in the BTD field, approximately +3 K, are circular and appear in the same location as the coldest values of the IRw around the cold ring. Alternatively, as indicated by radiative transfer model (RTM) simulations (Lattanzio et al., 2006), some of the higher BTD values might also be attributed to scattering/emissivity effects above storms within thin cirrus layers (microphysical explanation). Thus, one of the challenges provided by the A-Train observations is to evaluate these two concepts.

Given the relatively small magnitudes of the BTDs, it is important to check the error characteristics of the MODIS brightness temperatures to make sure the BTDs are at least as large as the expected errors. The MODIS specifications (available here: http://mcst.gsfc.nasa.gov/calibration/information) show that the required noise-equivalent temperature difference of the 6.7 μm WV band is 0.25 K, and the noise-equivalent temperature difference of the 11.0 μm IRw band is 0.05 K. Therefore, observed MODIS horizontal BTD (WV-IRw) differences greater than ~0.3 K are outside of the noise threshold and should be considered "real."

In order to gain some insight on the LSM and thin cirrus effects on the BTD values, some basic RTM simulations were run for the Missouri case. The RTM used in these simulations is identical to that described in Setvák et al. (2008) and in Grasso and Greenwald (2004), and takes into account absorption by gases as well as absorption and scattering by cloud particles when calculating the expected brightness temperatures as observed from the various MODIS infrared channels. The observed sounding from Springfield (SGF) at 18 UTC on 6 May 2007 is shown in Fig. 1H, and the corresponding MLS-observed profiles above these storms are shown in Fig. 1I, closely matching the sounding profile. A warm layer exists just above the tropopause; this layer is important for the forthcoming sensitivity tests. For the simulations, an opaque ice cloud was placed at 198 K (or 14.1 km, near the tropopause). Table 1 shows the resulting brightness temperatures from the model at MODIS band 27 and 31, as well as their BTD.

The base case simulation uses the SGF sounding (Fig. 1H) without modifying the water vapor content or adding a thin cloud above. In the sounding, the warm layer just above the tropopause is relatively moist (but subsaturated), so the resulting BTD of 0.772 K suggests that above-anvil water vapor is absorbing some of the outgoing 6.8 μm radiation and re-emitting at a slightly warmer temperature. For the first sensitivity test, the water vapor content within the warm layer from 14.7 to 16.2 km was increased to a value near saturation, and brightness temperatures are found in the "Enhanced WV" row of Table 1. The 11.0 μm BT remains the same as in the base case, but the 6.8 μm BT increases slightly, resulting in a larger BTD. This result is consistent with the findings of Setvák et al. (2008), and shows that even at very low absolute moisture contents in the lower stratosphere, increases in WV can result in measurable BT increases in the water vapor channel.

For the final test, the WV content was returned to the base case value, but a thin cirrus cloud having a total 11.0 μm optical depth of 0.27 was placed within the same warm layer (14.7 to 16.2 km). Ice crystals are effective absorbers of radiation at both 6.8 and 11.0 μm, so the BTs at both MODIS band 27 and 31 increased (Table 1, bottom row). In fact, the 11.0 μm BT increased even more than the 6.8 μm BT, so the BTD was lower than in the base case. Several different cirrus cloud optical thicknesses were tested (not shown), but the one used in Table 1 exhibited the largest BTD. These results show that water vapor in a warm lower stratospheric layer will cause the 6.8 μm BT to increase while not affecting the 11.0 μm BT, but a thin cirrus cloud in the same layer will cause the 11.0 μm BT to increase more than the 6.8 μm BT.

It should be noted that the magnitudes of the BTDs in these simulations were lower than was observed (+3 K, see

Please cite this article as: Setvák, M., et al., A-Train observations of deep convective storm tops, Atmos. Res. (2012), doi:10.1016/j.atmosres.2012.06.020

Fig. 1D). This is because the top of the opaque anvil cloud in the model was placed exactly at the height of the tropopause. In reality, the OT regions of the storm likely extended to colder temperatures, which would serve to increase the temperature difference between the cloud top and the warm environmental lower stratosphere layer above. In such a situation, the resulting BTDs would necessarily become more positive (as shown in Setvák et al., 2008). However, the trends in the sensitivity tests performed here would still remain valid.

6. Summary and concluding remarks

The present study has shown that the A-Train satellites and their instruments can provide valuable information about fine structures and features observed at the tops of deep convective storms. Specific features of interest were overshooting tops (OTs), the cold-U/V signature, above anvil and "jumping" cirrus plumes, and convectively-generated gravity waves. Though many of these features have already been documented from past observations by other satellites and their instruments, data from the CloudSat CPR and CALIPSO CALIOP provide additional detailed insights that have not been previously available. Nevertheless, A-Train observations of these features are quite uncommon due to the time of the A-Train orbit, their small size and duration, and the very narrow field of view of the CALIOP and CPR.

We have shown that for proper interpretation of some of the small-scale features, it is essential to work with the CPR and CALIOP tracks as accurately as possible, taking into account namely the 3–5 km parallax shift of the ground tracks when projected at the storm-top levels. A simple plot of the CloudSat and CALIPSO tracks from their corresponding HDF files for the Missouri event would have indicated that these instruments observed two prominent OTs. After the parallax correction, it was shown that only the edge of one of these OT signatures was observed. The opposite occurred for the Mexico event where it would have appeared that the profiling instruments missed an OT, but after properly accounting for parallax, it was found that they actually sampled the region with the coldest IR temperatures and peak height. The optical thickness of the convective anvil cloud was also shown to have a significant impact on the apparent cloud top height depicted by the CPR and CALIOP. This calls into question the definition of a "cloud top" in that the height of a "cloud top" strongly depends on the instrument that observes the cloud.

A storm exhibiting a cold-U feature was documented, showing the elevated nature of its embedded warm area as compared to the cold arms of the cold-U. A-Train observations of a cold-ring feature showed that there was no direct link between the cloud-top height and its IR brightness temperature. These two cases illustrate that the interpretation of warm areas inside cold-U and cold-ring features may differ from case to case, and further studies of similar cases are needed to better understand these phenomena. Another case featured distinct jumping cirrus, thin above anvil cirrus plumes, and gravity waves spreading from an active OT area.

Among the other features, the BTD (WV-IRw) field from MODIS was examined in detail for several events. The characteristics of the BTD field differed significantly from case to case. The BTD did not show any indication of the thin cirrus layers observed by CALIOP above several of the storm tops. The lack of signal in these situations implies that the higher BTD values are likely either related to stratospheric moisture or from the storm top microphysics. Also, the cases shown above illustrate ambiguity with regards to the correlation between the BTD and IRw BT fields; in one case (Missouri), high BTD values were associated with the coldest pixels, in other cases (e.g. Brazil or Australia) it was just the opposite — the higher BTD values were found above warmer regions of the storm. This variability should be considered when using this BTD within various objective algorithms such as OT or precipitating cloud detection. A radiative transfer model simulation was used to explore the sensitivity of the Missouri case to an increase in water vapor content or a thin cirrus cloud above the storm top. These results show that water vapor in a warm lower stratospheric layer will cause the WV BT to increase while not affecting the IRw BT, but a thin cirrus cloud in the same layer will cause the IRw BT to increase more than the WV BT, thereby diminishing the BTD magnitude.

In future studies using the A-Train data, we plan to aim specifically at two areas: 1) studies of additional cases with cold-U/V or cold-ring features and their embedded warm areas to further investigate the "plume masking mechanism" and 2) more complex studies of the BTD field including additional RTM simulations and simultaneous observations by MODIS and available geostationary satellites. Though the present study was simply focused on highlighting the A-Train observations and vertical structure depicted by the profiling instruments for the features discussed above, we are aware that the CPR and CALIOP offer additional opportunity for more detailed and quantitative investigation of the deep convective cloud tops. We hope that we and the rest of the community will continue to explore the cases documented here in much greater detail.

Finally, we plan to carry on the present A-Train storm-top studies with the EarthCare cloud radar and lidar (http://www.esa.int/esaLP/LPearthcare.html) which could be considered a follow-up mission to the A-Train satellites based on this payload after the launch of EarthCare around 2017. We also plan to examine storm stop signatures using the Visible Infrared Imaging Radiometer Suite (VIIRS) aboard the new generation of polar orbiting satellites such as Suomi NPP and JPSS. The GOES-R Advanced Baseline Imager (ABI, scheduled launch in 2015) and the Meteosat Third Generation Flexible Combined Imager (FCI, scheduled launch in 2017) can provide IR imagery at relatively high spatial resolution (2 km) but more importantly, very high temporal resolution ranging from 30 s for the ABI to 2.5 min for the FCI. This will allow us to advance our knowledge of the storm-top signatures examined in this paper as we will also be able to perform detailed studies of their temporal evolution which is not really possible with current geostationary instruments.

Acknowledgments

The authors wish to acknowledge Mike Fromm (Naval Research Laboratory, Washington, D.C.) and Louie Grasso (Cooperative Institute for Research in the Atmosphere, Ft. Collins, CO) for their valuable comments, suggestions and/or long-term support of this study, as well as NASA, NOAA and EUMETSAT for their data used in this study. Parts of

this research were carried out under support of the Grant Agency of the Czech Republic, project 205/07/0905; Grant SVV-2011-263308 of the Faculty of Mathematics and Physics of the Charles University, Prague, Czech Republic; Grant NSF ATM-0729898; and Grant C/SSAI/ASAP 2010 Program, Contract # 2626-08-021 Task 1-020CY4.

The views, opinions, and findings in this report are those of the authors, and should not be construed as an official CHMI, EUMETSAT, NOAA and or U.S. Government position, policy, or decision.

References

Ackerman, S.A., 1996. Global satellite observations of negative brightness temperature differences between 11 and 6.7 micron. J. Atmos. Sci. 53, 2803–2812.

Adler, R.F., Fenn, D.D., 1979. Thunderstorm intensity as determined from satellite imagery. J. Appl. Meteorol. 18, 502–517.

Adler, R.F., Mack, R.A., 1986. Thunderstorm cloud top dynamics as inferred from satellite observations and a cloud top parcel model. J. Atmos. Sci. 43, 1945–1960.

Adler, R.F., Markus, M.J., Fenn, D.D., Szejwach, D., Shenk, W.E., 1983. Thunderstorm top structure observed by aircraft overflights with an infrared radiometer. J. Appl. Meteorol. Climatol. 22, 579–593.

Adler, R.F., Markus, M.J., Fenn, D.D., 1985. Detection of severe Midwest thunderstorms using geosynchronous satellite data. Mon. Weather Rev. 113, 769–781.

Bedka, K.M., Brunner, J., Dworak, R., Feltz, W., Otkin, J., Greenwald, T., 2010. Objective satellite-based overshooting top detection using infrared window channel brightness temperature gradients. J. Appl. Meteorol. Climatol. 49, 181–202.

Bedka, K.M., Brunner, J., Dworak, R., Feltz, W., 2011. Objective satellite-base overshooting top and enhanced-V/cold ring detection: validation and relationships with severe weather. 6th European Conference on Severe Storms. Palma De Mallorca, Spain. 3–7 October 2011. Available online at: , http://www.essl.org/ECSS/2011/programme/abstracts/200.pdf.

Bedka, K.M., Dworak, R., Brunner, J., and Feltz, W., in press. Validation of satellite-based objective overshooting cloud top detection methods using CloudSat Cloud Profiling Radar observations. J. Appl. Meteorol. Climatol.

Dworak, R., Bedka, K.M., Brunner, J., Feltz, W., 2012. Comparison between GOES-12 overshooting top detections, WSR-88D radar reflectivity, and severe storm reports. Wea. Forecasting 27, 684–699, http://dx.doi.org/10.1175/WAF-D-11-00070.1.

Fritz, S., Laszlo, I., 1993. Detection of water vapor in the stratosphere over very high clouds in the tropics. J. Geophys. Res. 98 (D12), 22959–22967.

Fujita, T.T., 1982. Principle of stereoscopic height computations and their applications to stratospheric cirrus over severe thunderstorms. J. Meteorol. Soc. Jpn. 60, 355–368.

Grasso, L.D., Greenwald, T., 2004. Analysis of 10.7 μm brightness temperatures of a simulated thunderstorm with two-moment microphysics. Mon. Weather Rev. 132, 815–825.

Hasler, A.F., 1981. Stereographic observations from geosynchronous satellites—an important new tool for the atmospheric science. Bull. Am. Meteorol. Soc. 62, 194–212.

Heymsfield, G.M., Blackmer Jr., R.H., 1988. Satellite-observed characteristics of Midwest severe thunderstorm anvils. Mon. Weather Rev. 116, 2200–2224.

Heymsfield, G.M., Blackmer Jr., R.H., Schotz, S., 1983a. Upper level structure of Oklahoma tornadic storms on 2 May 1979, Pt. 1 radar and satellite observations. J. Atmos. Sci. 40, 1740–1755.

Heymsfield, G.M., Szejwach, G., Schotz, S., Blackmer Jr., R.H., 1983b. Upper level structure of Oklahoma tornadic storms on 2 May 1979, Pt. 2 proposed explanation of "V" pattern and internal warm region in infrared observations. J. Atmos. Sci. 40, 1756–1767.

Heymsfield, G.M., Fulton, R., Spinhirne, J.D., 1991. Aircraft overflight measurements of Midwest severe storms: implications on geosynchronous satellite interpretations. Mon. Weather Rev. 119, 436–456.

Iršič Žibert, M., Žibert, J., this issue. Monitoring and automatic detection of the cold-ring patterns atop deep convective clouds using Meteosat data. Atmos. Res.

Joyce, R.J., Janowiak, J., Huffman, G., 2001. Latitudinally and seasonally dependent zenith-angle corrections for geostationary satellite IR brightness temperatures. J. Appl. Meteorol. 40, 689–703.

Lattanzio, A., Watts, P.D., Govaerts, Y., 2006. Physical interpretation of warm water vapour pixels. EUMETSAT Technical Memorandum, 14. Available from , http://www.eumetsat.int/.

Levizzani, V., Setvák, M., 1996. Multispectral, high-resolution satellite observations of plumes on top of convective storms. J. Atmos. Sci. 53, 361–369.

Mace, G.G., Marchand, R., Stephens, G.L., 2007. Global hydrometeor occurrence as observed by CloudSat: initial observations from summer 2006. Geophys. Res. Lett. 34, L09808, http://dx.doi.org/10.1029/2006GL029017.

Mace, G.G., Zhang, Q.Q., Vaughan, M., Marchand, R., Stephens, G., Trepte, C., Winker, D., 2009. A description of hydrometeor layer occurrence statistics derived from the first year of merged Cloudsat and CALIPSO data. J. Geophys. Res. 114, D00A26, http://dx.doi.org/10.1029/2007JD009755.

Mack, R.A., Hasler, A.F., Adler, R.F., 1983. Thunderstorm cloud top observations using satellite stereoscopy. Mon. Weather Rev. 111, 1949–1964.

McCann, D.W., 1983. The enhanced-V: a satellite observable severe storm signature. Mon. Weather Rev. 111, 887–894.

Mills, P., Astling, E., 1977. Detection of tropopause penetrations by intense convection with GOES enhanced infrared imagery. Preprints 10th Conf. Severe Local Storms: Amer. Meteor. Soc. , pp. 61–64.

Minnis, P., Yost, C.R., Sun-Mack, S., Chen, Y., 2008. Estimating the top altitude of optically thick ice clouds from thermal infrared satellite observations using CALIPSO data. Geophys. Res. Lett. 35, L12801, http://dx.doi.org/10.1029/2008GL033947.

Negri, A.J., 1982. Cloud-top structure of tornadic storms on 10 April 1979 from rapid scan and stereo satellite observations. Bull. Am. Meteorol. Soc. 63, 1151–1159.

Purdom, J.F.W., 1976. Some uses of high-resolution GOES imagery in the mesoscale forecasting of convection and its behavior. Mon. Weather Rev. 104, 1474–1483.

Putsay, M., Simon, A., Szenyán, I., Kerkmann, J., Horváth, G., 2011. Case study of the 20 May 2008 tornadic storm in Hungary — remote sensing features and NWP simulation. Atmos. Res. (ISSN: 0169-8095) 100, 657–679, http://dx.doi.org/10.1016/j.atmosres.2010.08.008.

Putsay, M., Simon, A., Setvák, M., Szenyán, I., Kerkmann, J., 2012. Simultaneous observation of above-anvil ice plume and plume-shaped BTD anomaly atop a convective storm. Atmos. Res. (accepted for this issue).

Rodriguez, A., Marcos, C., 2010. Algorithm theoretical basis document for EUMETSAT Nowcasting Satellite Applications Facility "Convective Rain Rate" productAvailable online at: , http://www.nwcsaf.org/indexScientificDocumentation.html2010.

Schlesinger, R.E., 1984. Mature thunderstorm cloud-top structure and dynamics: a three-dimensional numerical simulation study. J. Atmos. Sci. 41, 1551–1570.

Schlesinger, R.E., 1988. Effects of stratospheric lapse rate on thunderstorm cloud-top structure in a three-dimensional numerical simulation. Part I: some basic results of comparative experiments. J. Atmos. Sci. 45, 1555–1570.

Schmetz, J., Tjemkes, S.A., Gube, M., van de Berg, L., 1997. Monitoring deep convection and convective overshooting with METEOSAT. Adv. Space Res. 19, 433–441.

Setvák, M., Rabin, R.M., 2003. MODIS observations of deep convective cloud tops. Proc. The 2003 EUMETSAT Meteorological Satellite Conference, Weimar, Germany: EUM1011-3932, P39. ISBN: 92-9110-064-1, pp. 381–388.

Setvák, M., Lindsey, D.T., Rabin, R.M., Wang, P.K., Demeterova, A., 2008. Indication of water vapor transport into the lower stratosphere above midlatitude convective storms: Meteosat Second Generation satellite observations and radiative transfer model simulations. Atmos. Res. 89/1-2, 170–180.

Setvák, M., Lindsey, D.T., Novák, P., Wang, P.K., Radová, M., Kerkmann, J., Grasso, L., Su, S.-H., Rabin, R.M., Šťástka, J., Charvát, Z., Kyznarová, H., 2010. Cold-ring-shaped cloud top features atop convective storms. Atmos. Res. (ISSN: 0169-8095) 97, 80–96, http://dx.doi.org/10.1016/j.atmosres.2010.03.009.

Shenk, W.E., 1974. Cloud top height variability of strong convective cells. J. Appl. Meteorol. 13, 917–922.

Šťástka, J., Radová, M., 2012. Detection and analysis of anomalies in the brightness temperature difference field using MSG rapid scan data. Atmos. Res., http://dx.doi.org/10.1016/j.atmosres.2012.05.015

Stephens, G.L., Vane, D.G., Boain, R.J., Mace, G.G., Sassen, K., Wang, Z., Illingworth, A.J., O'Connor, E.J., Rossow, W.B., Durden, S.L., Miller, S.D., Austin, R.T., Benedetti, A., Mitrescu, C., the CloudSat Science Team, 2002. The CloudSat mission and the A-Train. A new dimension of space-based observations of clouds and precipitation. Bull. Am. Meteorol. Soc. 83, 1771–1790.

van Hees, R.M., Lelieveld, J., Collins, W.D., 1999. Detecting tropical convection using AVHRR satellite data. J. Geophys. Res. 104, 9213–9228, http://dx.doi.org/10.1029/1998JD200079.

Wang, P.K., 2007. The thermodynamic structure atop a penetrating convective thunderstorm. Atmos. Res. 83, 254–262.

Wang, P.K., Setvak, M., Lyons, W., Schmid, W., Lin, H., 2009. Further evidence of deep convective vertical transport of water vapor through the tropopause. Atmos. Res. 94, 400–408.

Please cite this article as: Setvák, M., et al., A-Train observations of deep convective storm tops, Atmos. Res. (2012), doi:10.1016/j.atmosres.2012.06.020